

PART II

GEOPHYSICAL SURVEY

(IP ELECTRIC SURVEY)

1. SUMMARY OF SURVEY

The survey was carried out in the Mina la Morena area as a part of the Phase IV survey to obtain geophysical information regarding the subsurface structures, mineralized zones and ore deposits.

The electric survey of IP method was conducted to ascertain the size of mineralized zone or zones in the area and to get the information for selecting the drilling targets.

2. OUTLINE OF SURVEY

2.1 Configuration of Survey Lines and Points

The survey lines and points are shown in PL. II-1 (LOCATION MAP OF IP SURVEY LINES AND POINTS).

2.2 Quantity of Survey

Area covered	3.3 km ²
Total line length	34.9 km
Number of lines	23
Length of each line	1.5 km (Partly, 0.7, 1.1, 1.1, 1.8, and 2.0 km)
Line spacing	100 m
Separation of points	100 m
Electrode configuration	Dipole-dipole
Coefficient of electrode separation	n=1, 2, 3, 4

2.3 Instruments

Transmitter

Type :	IPC-7/15 KW
Maker :	SCINTREX (CANADA) LTD.
Output voltage :	0 ~ 5000 V, DC
Output current :	0 ~ 20A, DC

Receiver

Type :	IPR-8
Maker :	SCINTREX (CANADA) LTD.
Maximum sensitivity range :	0.3 mV
Chargeability range	0 ~ 100 milli-seconds

Generator

Type :	MG 15 KW-AC
Maker :	SCINTREX (CANADA) LTD.
Output :	15 KW, 400 Hz, 300V

2.4 Setting of Survey Lines

Line setting was carried out using transit and measuring tape. Survey points were set with an interval of 100 m in horizontal distance, which were marked by the posts with numbering on it. Survey lines were set in N56°W with 100 m spacing. In order to investigate the anomalies in detail which were detected at the end of the lines, additional two survey lines of L-B and L-C were set. Survey lines of L-3, L-4 and L-5 were extended to the northwest, and those of L-5, L-6, L-13, L-15 and L-16 to the southeast.

3. SURVEY METHOD

Time Domain Induced Polarization Method was applied for the IP electric survey.

When direct current is let to flow intermittently in the rock containing electric conductive minerals such as ore deposit and mineralized zone, charge and discharge phenomena are observed at the interface between the rock and the electric conductive minerals.

The discharge voltage called dischargeability is measured in the time domain method.

The wave forms of the primary current and the measured voltage are shown in Fig. II-1. Six integrated values of transient voltage such as M_{61} , M_{62} , M_{63} , M_{64} , M_{65} and M_{66} with intervals from 0.13 to 0.26 seconds were measured 0.13 seconds after primary current was cut off as shown in the figure. These integrated values are called chargeability and expressed in the unit of milli-second.

Dipole-dipole array as shown in Fig. II-2 was used as configuration of electrode for the measurement of chargeability.

If electrode distance is represented by a and coefficient of electrode separation by n , then the distance between current electrode and potential electrode becomes $n \cdot a$. Consequently, the increase in coefficient of electrode separation results in the increase in depth of measurement. In this survey, the electrical information was obtained at the depths corresponding to $n=1, 2, 3, 4$. In this array, two seconds on and two seconds off pulse current as shown in Fig. II-1 was supplied repeatedly between current electrode C_1 and C_2 to measure both the electric potential when the current was on and the chargeability when the current was off at potential electrodes P_1 and P_2 .

In this survey, chargeability M , electric potential V , and supplied current I were measured, and apparent resistivity ρ_a was calculated from the measured values of V and I by the following formula:

$$\rho_a = K \frac{V}{I} (\Omega\text{-m}),$$

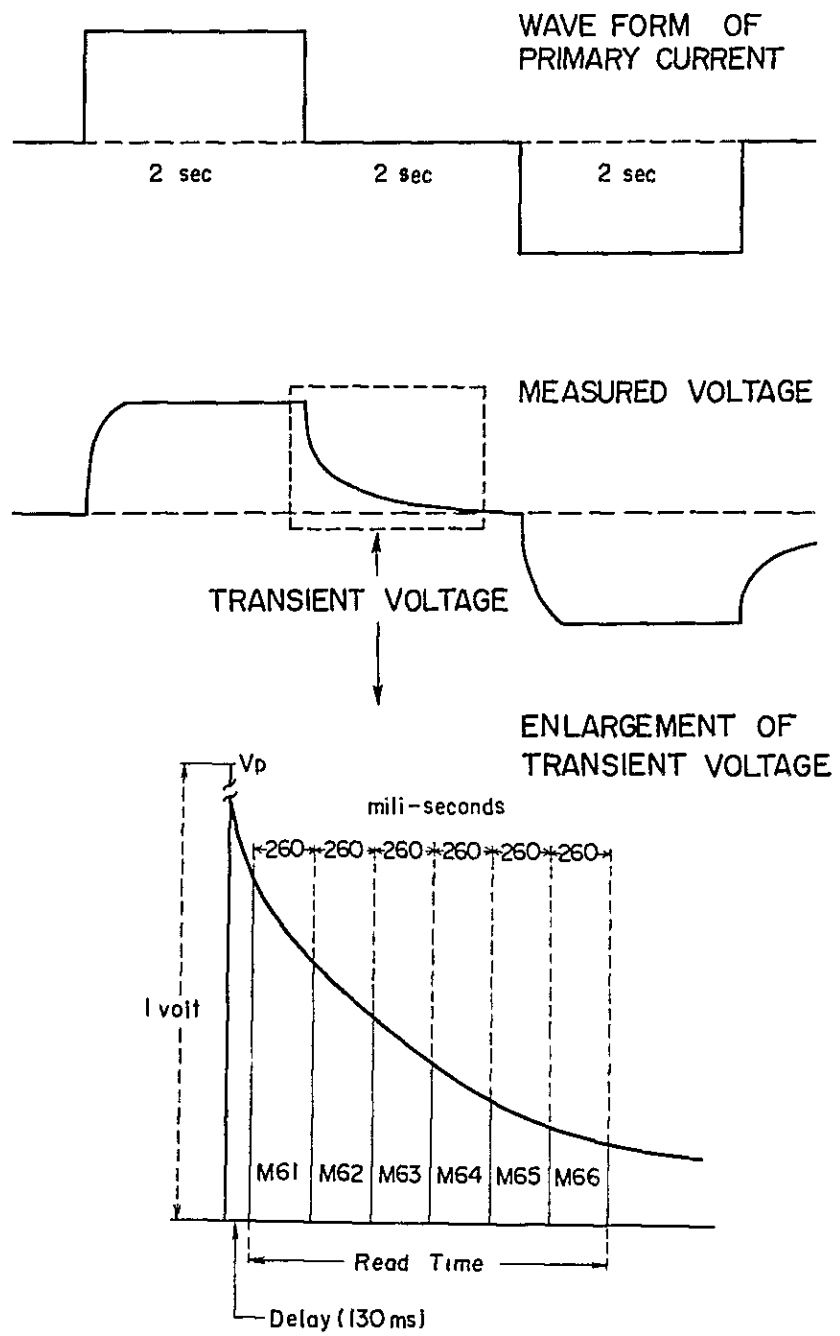
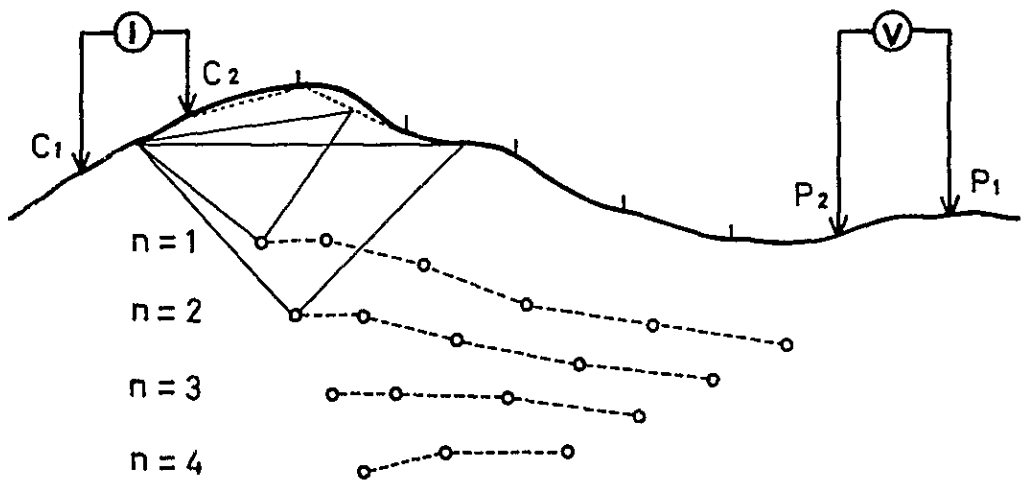
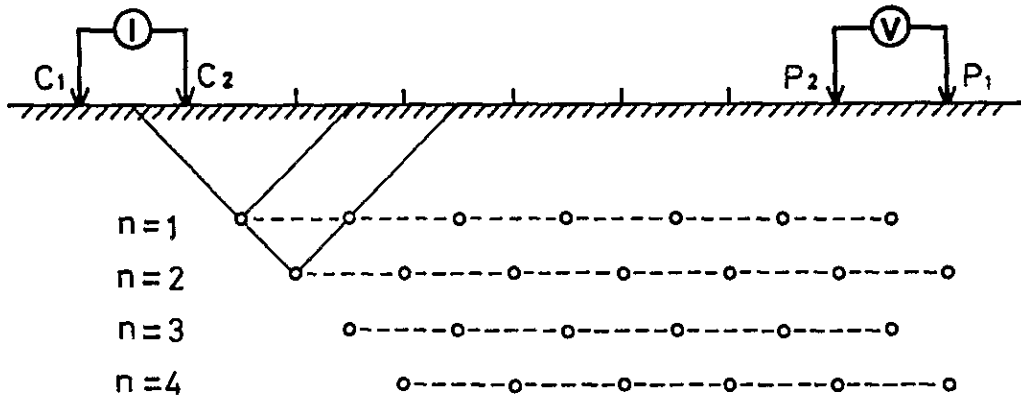
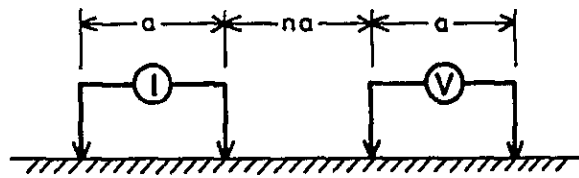


Fig II-1 Wave forms of primary current and measured voltage

Fig.II-2 Electrode configuration of dipole - dipole array



where $K = a \cdot \pi \cdot n(n+1)$: geometric coefficient
a : electrode distance
n : coefficient of electrode separation

Metal sulphides generally show lower specific resistivity and larger chargeability, so that the ratio between chargeability and apparent resistivity is used as an indicator showing the effect by metallic minerals which is called Apparent Metal Conduction Factor (abbreviated hereinafter as AMF) and defined by the following formula in this report:

$$AMF = \frac{M}{\rho_a} \times 1000 \text{ (milli-sec/ } \Omega\text{-m)}$$

The values of M, ρ_a , and AMF are indicated at the profiles as shown in Fig. II-2.

The term "IP anomaly" used hereunder is synonymous with the "chargeability anomaly" mentioned above.

•

4. ANALYSIS OF SURVEY RESULTS

The results of survey and calculation are shown in the plans such as PL. II-2 ~5 (MAP OF CHARGEABILITY, n=1, 2, 3, 4), PL. II-6 ~9 (MAP OF APPARENT RESISTIVITY, n=1, 2, 3, 4) and PL. II-10 ~13 (MAP OF APPARENT METAL FACTOR, n=1, 2, 3, 4), and in IP profiles (PL. II-14 ~19).

The analysis was made by making a qualitative study on the simulated results derived from subsurface IP models assumed from five survey lines to estimate the relationship between IP anomaly and the geology in the survey area.

4.1 Plan Analysis

4.1.1 Analysis of the Chargeability Plans

In the maps of chargeability (PL. II-2 ~5), the chargeability measured in the survey area shows minimum value of 5.5 milli-sec. and maximum value of 53.8 milli-sec., while a fairly wide part of the area is covered by low chargeability below 25 milli-sec. Accordingly, the values lower than 25 milli-sec. were considered to be background, and analysis was made on the basis that the values higher than 25 milli-sec. were IP anomalies. However, in some zones with values from 20 to 25 milli-sec., consideration was made in relation to the geology by investigating the maps of chargeability, n=1, 2, 3, 4.

IP anomalies were named as A(n-1), B(n-1), A(n-2), B(n-2)..... .

Analysis of survey results is described below.

(1) Chargeability plan (n=1) (See PL. II-2)

The name and chargeability range of each anomaly are as follows:
The magnitude of the anomalous area was classified qualitatively into three categories of "grand", "medium", and "small" for the purpose of comparison.

A(n-1) : 25 ~ 42.0 milli-sec. grand.

B(n-1) : 25 ~ 33.6 milli-sec. grand.

C(n-1) : 25 ~ 28.6 milli-sec. small.

D(n-1) : 25 ~ 25.2 milli-sec. small.

In the maps of n=2, 3, 4, no specific anomaly which corresponds to these anomalies was not detected and the anomalies are considered to be caused by small chargeable rock bodies at shallow depths.

E(n-1) : 20 ~ 21.8 milli-sec. small.

F(n-1) : 20 ~ 20.2 milli-sec. small.

G(n-1) : 20 ~ 20.2 milli-sec. small.

H(n-1) : 20 ~ 23.0 milli-sec. small.

I(n-1) : 20 ~ 24.0 milli-sec. small.

(2) Chargeability plan (n=2) (See PL. II-3)

A(n-2) : 25 ~ 43.7 milli-sec. grand. This anomaly is located in almost the same place with A(n-1). Although the area is a little larger than A(n-1), the maximum value of anomaly is almost the same.

B(n-2) : 25 ~ 35.3 milli-sec. grand. The anomaly is located in almost the same place with B(n-1). Although the maximum value is almost the same to B(n-1), the area of anomaly is a little larger.

C(n-2) : 25 ~ 28.6 milli-sec. small. The anomaly is located close to C(n-1).

E(n-2) : 25 ~ 25.2 milli-sec. small. The anomaly is in the neighborhood of E(n-1).

F(n-2) : 25 ~ 26.0 milli-sec. small. The anomaly is in the neighborhood of F(n-1).

G(n-2) : 25 ~ 29.0 milli-sec. small. The anomaly is close to G(n-1).

H(n-2) : 25 ~ 31.9 milli-sec. small. The anomaly is in the same place with H(n-1).

I(n-2) : 25 ~ 26.0 milli-sec. small. This anomaly was not detected in the plan of n=1, and it is considered to be an anomaly caused by a chargeable rock body occurring at the depth more than 100 meters below the surface.

J(n-2) : 20 ~ 24.4 milli-sec. medium. Like I(n-2), this anomaly was not detected in the plan of n=1.

(3) Chargeability plan (n=3) (See PL. II-4)

AB(n-3) : 25 ~ 37.0 milli-sec. grand. This anomaly is wide and is likely to be formed by the combination of two anomalies of A(n-1) and B(n-1), or A(n-2) and B(n-2) which were observed on the maps of n=1, 2 when taken the extent of distribution into consideration, and it has a very complicated shape.

C(n-3) : 25 ~ 25.2 milli-sec. small. It is in the same place with C(n-2).

E(n-3) : 25 ~ 26.9 milli-sec. small. It is located close to E(n-2).

F(n-3) : 25 ~ 26.9 milli-sec. small. It is in the neighborhood of F(n-2).

Any anomaly which corresponds to G or H on maps of n=1, 2 was not detected on the maps of n=3, 4.

I(n-3) : 25 ~ 37.0 milli-sec. medium. It is almost in the same place with I(n-2), and the extent of anomaly is greater than that.

J(n-3) : 25 ~ 29.8 milli-sec. small.

K(n-3) : 25 ~ 27.3 milli-sec. small.

J(n-3) is in the same place with J(n-2), and the area of anomaly is approximately one fourth of J(n-2). K(n-3) is located close to the north end of J(n-2).

L(n-3) : 25 ~ 28.6 milli-sec. small.

M(n-3) : 25 ~ 29.4 milli-sec. small.

These two anomalies are found only on this plan, and, therefore, they are considered to be the anomalies caused by small chargeable rock bodies.

N(n-3) : 25 ~ 28.6 milli-sec. medium. This anomaly has a elongated shape and is located along northeastern periphery of A(n-2).

(4) Chargeability plan (n=4) (See PL. II-5)

AB(n-4) : 25 ~ 40.3 milli-sec. grand. The anomaly is distributed almost in the same place with AB(n-3). The extent of its distribution

is narrower than AB(n-3), and is more complicated in the shape. It is apparent from the form of distribution that the anomaly AB(n-3) and AB(n-4) are continuously stretching along the survey line L-C from survey point 300 to 1000 on it. However, the survey line L-C is a short additional survey line from survey point 800 to the point 1500 in which the segment from 0 to 800 is not contained. Therefore, because of the absence of the data over the segment and another survey line to the south of the line, it is difficult to assume the shape and extent of these anomalies.

C(n-4) : 25 ~ 27.9 milli-sec. medium. It is located almost in the same place with C(n-3), and its extent is approximately three times as large as that of C(n-3).

E(n-4) : 25 ~ 31.9 milli-sec. medium. It is located almost in the same place with E(n-3), and its extent is approximately three times as large as that of E(n-3).

Any anomaly which corresponds to the F anomaly detected on each plan of n=1, 2, and 3 was not found in this plan.

I(n-4) : 25 ~ 33.6 milli-sec. medium. The anomaly corresponds to I(n-3).

J(n-4) : 25 ~ 33.6 milli-sec. medium. It corresponds to J(n-2), J(n-3), and K(n-3).

Any anomaly which corresponds to L, M, and N anomaly detected on the plan of n=3 was not found on this plan.

O(n-4) : 25 ~ 53.8 milli-sec. grand. It is an anomaly that was not found on each plan of n=1, 2 and 3. It has a wide extent of distribution having the highest value of anomaly measured within the survey area. These features lead to estimate the presence of a rock body with high chargeability at the depth deeper than 250 m from the surface.

P(n-4) : 25 ~ 33.6 milli-sec. small.

Q(n-4) : 25 ~ 25.2 milli-sec. small.

These anomalies were also found on this map for the first time, and

it is assumed that it would be caused by the rock body with high chargeability emplaced at the approximate depth of 250 m which corresponds to coefficient $n=4$.

As described above, sometimes the anomalies are found approximately in the same places, and some anomalies are found only on the peculiar plan or plans. These features are summarized in Table II-1 (Measured chargeability anomalies).

Table II-1 Measured chargeability anomalies

Name of anomaly	n = 1		n = 2		n = 3		n = 4	
	Magnitude	Max.value	Mag.	Max.v	Mag.	Max.v	Mag.	Max.v
A	◎	42.0	◎	43.7	} ◎	37.0	◎	40.3
B	◎	33.6	◎	35.3				
C	○	28.6	○	28.6	○	25.2	○	27.9
D	○	25.2	-	-	-	-	-	-
E	○	21.8	○	25.2	○	26.9	○	31.9
F	○	20.2	○	26.0	○	26.9	-	-
G	○	21.0	○	29.0	-	-	-	-
H	○	23.0	○	31.9	-	-	-	-
I	○	24.0	○	26.0	○	37.0	○	33.6
J			○	24.4	○	29.8	○	33.6
K					○	27.3	-	-
L					○	28.6	-	-
M					○	29.4	-	-
N					○	28.6	-	-
O							◎	53.8
P							○	33.6
Q							○	25.2

Magnitude: ◎=grand, ○=medium, o=small.

Unit: milli-seconds

Anomalies depicted on the chargeability plans, geology, and results of diamond drilling are correlated and summarized in Table II-2 (Geologic explanation of chargeability anomalies).

Table II-2 Geologic explanation of chargeability anomalies

Name of Anomaly	n				Geologic explanation
	1 100m	2 150m	3 200m	4 250m	
A	⊙	⊙	} ⊙	⊙	Muddy layer which contains sulfide and/or carbonaceous matter, upper than Kau IX layer.
B	⊙	⊙			
C	o	o	o	○	Parts which contain sulfide and/or carbonaceous matter in Kau VII and IX.
D	o	-	-	-	Small part rich in carbonaceous matter, near ground surface
E	o	o	o	○	Parts in Kau VII and IV
F	o	o	o	-	Mineralized zone(?), fault(?)
G	o	o	-	-	Muddy calcareous part in Kau III(?) or fault(?)
H	o	o	-	-	Muddy calcareous part in Kau VII
I	o	o	○	○	Muddy calcareous part in Kau III
J		○	o	○	Same as above
K			o	-	Same as above
L			o	-	Mineralized zone(?), fault(?)
M			o	-	Fault(?), mineralized zone(?)
N			○	-	Muddy calcareous part in Kau IX
O				⊙	Parts rich in sulfide or carbonaceous matter in Kau IX and XI
P				o	Carbonaceous part in Kau V
Q				o	Muddy calcareous part in Kau III

⊙ : grande, ○ : medium, o : small in scale.

4.1.2 Analysis of Maps of Apparent Resistivity

It is readily understood that the apparent resistivity in the survey area has significantly high values by reference to the maps of apparent resistivity. For the purpose of examining the relationship between apparent resistivity ρ_a and chargeability M, chargeability anomalies depicted on maps of chargeability of $n = 1 \sim 4$ as described above were transferred to maps of apparent resistivity of $n = 1 \sim 4$. Average value of ρ_a in whole survey area and that in each anomalous zone were calculated for each of n, and summarized in Table II-3 (Average of apparent resistivity in anomalous zone of chargeability).

Table II-3 Average of apparent resistivity in anomalous zones of chargeability

Name of Anomaly	n M, Av	n = 1		n = 2		n = 3		n = 4	
		M	5,300*	M	4,800*	M	5,100*	M	4,900*
A	⊖	1,890	⊖	1,980	⊖	2,700	⊖	1,870	
B	⊖	2,270	⊖	3,070					
C	○	4,150	○	1,460	○	2,080	○	1,690	
D	○	910							
E	○	5,660	○	4,110	○	1,830	○	1,360	
F	○	12,400	○	6,470	○	12,200			
G	○	6,910	○	2,200					
H	○	9,520	○	12,500					
I	○	2,390	○	1,450	○	1,010	○	2,000	
J			○	3,100	○	3,870	○	3,200	
K					○	1,000			
L					○	9,610			
M					○	6,100			
N					○	1,300			
O							○	2,470	
P							○	2,830	
Q							○	3,300	
(A)		53,407		81,996		36,442		27,018	
(B)		165		228		141		228	
(A) ÷ (B)		324 (2)		360 (1)		258 (3)		119 (4)	

M=Magnitude, ⊖=grand, ○=medium, ◦=small. Av=Average value. Unit: Ω-m
 *: Average of measured values in n=1, 2, 3, 4 respectively. (A) is maximum and (B) is minimum of measured values in n=1, 2, 3, 4 respectively.
 ①, ②, ... is order of magnitude of (A) ÷ (B)

By studying the maps of apparent resistivity and Table II-3, following characteristics can be summarized.

- (1) Average value of all measured values of ρ_a is 5,000 Ω -m, and the average of measured values of ρ_a for each of n can also be regarded to be approximately 5,000 Ω -m.
- (2) The pattern of distribution of apparent resistivity is most complicated in the map of n=2, and becomes a little more simplified in successive order of n=1, 3, and 4, which correspond to the order of magnitude of the ratio between measured maximum and minimum values of ρ_a .
- (3) The zones of distribution of ρ_a higher than 5,000 Ω -m correspond roughly to the recrystallized zone in the survey area.
- (4) Large-scale anomalies of chargeability (marked as \odot and \circ in Table II-2 and Table II-3) are distributed in low ρ_a zones around the recrystallized zone.
- (5) From Table II-3, it can be said that the number of anomalous zones of chargeability in which average value of ρ_a is smaller than that in the whole survey area (5,000 Ω -m) increases as the value of n increases.
- (6) In particular, the average values of ρ_a in anomalous zones of chargeability at n=4 are all smaller than the average value of ρ_a in the whole survey area.
- (7) The number of anomalous zones of chargeability detected on the maps is 36, and it can be said that (number of chargeability anomalies having the average ρ_a lower than 5,000 Ω -m): (number of chargeability anomalies having the average ρ_a higher than 5,000 Ω -m) = 27:9 = 3:1, and that the chargeability anomalies are generally distributed in the zones of lower ρ_a .
- (8) Especially all of fourteen large-scale anomalies (marked as \odot and \circ) have the range of average ρ_a values (1,000 ~ 3,200 Ω -m) fairly smaller than the average value in the whole survey area.
- (9) Small-scale anomalies (marked as \circ) have higher average values of ρ_a , and are mostly distributed in the recrystallized zone.

- (10) Among the chargeability anomalies, those distributed in the zones of lower ρ_a value are classified as type A, and those in the higher ρ_a value as type B. It is estimated by correlating these ρ_a values with geology and the drilling results that A type anomalies are caused by fine-grained sulfide minerals in limestone or pelitic beds containing carbonaceous matter, and B type anomalies are caused by ore deposits or mineralized zones.
- (11) From the circumstances described in (6) and (10), it is assumed that the more abundant sulfide mineral and carbonaceous matter would be contained specially in the strata which correspond to the anomalies having the coefficient of $n=4$.
- (12) There are some parts in which chargeability anomalies have not been detected notwithstanding the very low apparent resistivities. This is presumably due to the effect of carbonaceous matter or water in the absence of sulfide minerals.

4.1.3 Analysis of Maps of Apparent Metal Factor

As described in chapter 3, Apparent Metal Factor is defined as follows:

$$AMF = \frac{M}{\rho_a} \times 1,000 \text{ (milli-sec}/\Omega\text{-m)}$$

As can be readily understandable from the formula, the value of AMF will be large in anomalies where chargeability M is high and apparent resistivity ρ_a is low as found in A-type anomalies mentioned above, while AMF will be small in B-type anomalies.

The characteristics common to each of the maps of $n=1, 2, 3$ and 4 (PL. II-10 ~ 13) are:

- (1) The zones with larger values of AMF roughly coincide with the zones in which M is large and ρ_a is small.
- (2) In some parts, large values of AMF were calculated while M is small, and this is due to very small ρ_a . It is assumed that such parts would coincide with the parts rich in carbonaceous matter or water as stated in 4-1-2.

- (3) Anomalous zones of AMF are distributed surrounding the recrystallized zone in the survey area, and no AMF anomaly was found within the recrystallized zone.

4.2 Profile Analysis

The results of the profile analysis for chargeability, apparent resistivity and apparent metal factor of each survey line coincide with those of the plan analysis in many cases. Here, the results of the profile analysis are summarized in Table II-4 (Results of profile analysis) correlated with the results of plan analysis.

Table II-4 Result of profile analysis

Line	Chargeability M(milli-sec)	Name of anomaly in each map of chargeability	Apparent resistivity $\rho_a(\Omega\text{-m})$	Apparent metal factor MF ($\frac{\text{sec}}{\Omega\text{-m}}$)
L-C	25.0 ~ 27.5	AB	High ρ_a below SP. 700~800	Anomaly below SP. 1,000~1,100
L-B	25.0 ~ 46.3	A, B, AB	Low ρ_a below SP. 600~1,300	Anomaly below SP. 800~1,000
L-A	25.0 ~ 40.3	A, B, AB, O	Low ρ_a between SP. 400 and 1,300	Anomaly below SP. 1,000~1,100
L-O	25.0 ~ 43.7	A, B, AB, O	Low ρ_a as a whole except SP. 300~400	Anomaly below SP. 600 ~ 700
L-1	25.0 ~ 33.6	A, B, AB, O	ρ_a distribution is complicated a little.	
L-2	25.0 ~ 29.4 25.0 ~ 33.6	A, N AB	Low ρ_a between SP. 500 and 1,200	Anomaly SP. 900~1,200
L-3	25.0 ~ 25.2 25.0 ~ 53.8	N O	Low ρ_a between SP. 400 and 1,100	Anomaly below SP. 400 ~ 500 and 1,200
L-4	25.0 ~ 37.0	O	Low ρ_a between SP. 500 and 1,100	Anomaly SP. 400 ~ 500 and 600 ~ 800
L-5	25.0 ~ 27.4	C, O, E	ρ_a pattern is complicated	
L-6	25.0 ~ 28.6 25.0 ~ 31.1	C O	Same as above	Weak anomaly coincides with C and O.
L-7	25.0 ~ 31.9	C, F, E	High ρ_a as a whole.	Weak anomaly coincides with C, F, E.
L-8	25.0 ~ 28.6	L	Same as above.	
L-9			Same as above.	
L-10			Same as above.	
L-11	25.0 ~ 33.6	P	ρ_a pattern is complicated.	Anomaly below SP. 200~300
L-12	25.0 ~ 29.4	M	Same as above	
L-13	25.0 ~ 29.0	G	High ρ_a below SP. 300~500 and 600~1,100.	
L-14			High ρ_a below SP. 300~500 and 700~1,200.	
L-15	25.0 ~ 33.6	I, Q, J	High ρ_a in the center and lower part of the survey line.	
L-16	25.0 ~ 37.0	I, J	Low ρ_a as a whole	Anomaly below SP. 1,400~1,500
L-17	25.0 ~ 33.6	J, K	Same as above.	Anomaly below SP. 900~1,000
L-18			Same as above.	
L-19	25.0 ~ 31.9	H	Same as above.	

Table II-4 Result of profile analysis

SP.= Survey Point

Line	Chargeability M(milli-sec)	Name of anomaly in each map of chargeability	Apparent resistivity $\rho_a(\Omega\text{-m})$	Apparent metal factor AMF ($\frac{\text{sec}}{\Omega\text{-m}}$)	Remarks
L-C	25.0 ~ 27.5	AB	High ρ_a below SP. 700~800	Anomaly below SP. 1,000~1,100	Patterns of anomaly of M, ρ_a , and AMF are simple.
L-B	25.0 ~ 46.3	A, B, AB	Low ρ_a below SP. 600~1,300	Anomaly below SP. 800~1,000	High anomaly of M is located in same place of that of AMF.
L-A	25.0 ~ 40.3	A, B, AB, O	Low ρ_a between SP. 400 and 1,300	Anomaly below SP. 1,000~1,100	Lower part of anomaly A coincides with AMF anomaly.
L-O	25.0 ~ 43.7	A, B, AB, O	Low ρ_a as a whole except SP. 300~400	Anomaly below SP. 600 ~ 700	AMF anomaly coincides with lower part of B.
L-1	25.0 ~ 33.6	A, B, AB, O	ρ_a distribution is complicated a little.		
L-2	25.0 ~ 29.4 25.0 ~ 33.6	A, N AB	Low ρ_a between SP. 500 and 1,200	Anomaly SP. 900~1,200	AMF anomaly coincides with A and N.
L-3	25.0 ~ 25.2 25.0 ~ 53.8	N O	Low ρ_a between SP. 400 and 1,100	Anomaly below SP. 400 ~ 500 and 1,200	AMF anomaly coincides with N and O.
L-4	25.0 ~ 37.0	O	Low ρ_a between SP. 500 and 1,100	Anomaly SP. 400 ~ 500 and 600 ~ 800	AMF anomaly below SP. 400~500 coincides with anomaly O.
L-5	25.0 ~ 27.4	C, O, E	ρ_a pattern is complicated		
L-6	25.0 ~ 28.6 25.0 ~ 31.1	C O	Same as above	Weak anomaly coincides with C and O.	
L-7	25.0 ~ 31.9	C, F, E	High ρ_a as a whole.	Weak anomaly coincides with E.	It is inferred that high ρ_a zone coincides with recrystallized zone.
L-8	25.0 ~ 28.6	L	Same as above.		Same as above.
L-9			Same as above.		Same as above.
L-10			Same as above.		Same as above.
L-11	25.0 ~ 33.6	P	ρ_a pattern is complicated.	Anomaly below SP. 200~300	
L-12	25.0 ~ 29.4	M	Same as above		
L-13	25.0 ~ 29.0	G	High ρ_a below SP. 300~500 and 600~1,100.		
L-14			High ρ_a below SP. 300~500 and 700~1,200.		
L-15	25.0 ~ 33.6	I, Q, J	High ρ_a in the center and lower part of the survey line.		
L-16	25.0 ~ 37.0	I, J	Low ρ_a as a whole	Anomaly below SP. 1,400~1,500	AMF anomaly coincides with I.
L-17	25.0 ~ 33.6	J, K	Same as above.	Anomaly below SP. 900~1,000	AMF anomaly coincides with J.
L-18			Same as above.		
L-19	25.0 ~ 31.9	H	Same as above.		

5. IP SIMULATION

The survey area includes strongly anomalous zones of IP (chargeability), and a significantly high apparent resistivity zone which is considered to coincide with the recrystallized zone. Therefore, both IP and resistivity simulations were conducted on the three and two survey lines respectively as follows:

IP simulation: L-A, L-6 and L-17,

Resistivity simulation: L-8 and L-11.

Since the simulation of the time domain IP method used in this survey is theoretically impossible, simulation of the frequency domain IP method was carried out as a substitute and the results of the simulation were compared with the field data.

The frequency domain IP method is based on the principle that the resistivity of a medium with IP effect depends on the frequency of alternating current which is supplied to the medium. The IP effect thus produced is called Frequency Effect (FE) and is expressed by the following formula:

$$FE = \frac{\rho_L - \rho_H}{\rho_H} \times 100 (\%)$$

where, ρ_L : Resistivity in low frequency (Ω -m)

ρ_H : Resistivity in high frequency (Ω -m)

The simulation is performed by following procedure: At first, different resistivities (ρ_1, ρ_2) are given respectively to a medium of a certain shape with IP effect and to the surrounding medium without IP effect to find the apparent resistivity at each survey point. The varied resistivity (ρ_1) corresponding to a certain FE value is provided to the medium which has IP effect without varying the resistivity of the surrounding medium (ρ_2) to obtain apparent resistivity again at each survey point. By the use of these two sets of apparent resistivity thus obtained and from the formula given above, FE values are calculated for each survey point to make a contour map of the FE values. Finally, model and resistivity of underground structure are varied so as to make the contour map agree with the field data as closely as possible.

Since the time domain IP method differs from the frequency domain IP

method in the unit of measured value, conversion of the value by time domain method to that by frequency domain method is theoretically impossible. Sometimes, the use of data measured by these two methods at the same location will make it empirically possible. However this conversion can not easily be made actually because of a number of variables such as the frequency of the current in frequency domain IP method, time interval of square-wave current in time domain IP method, and the time range of integration of chargeability measurement.

Since this procedure has various problems as mentioned above, the underground structure was finally adopted in this simulation when the contour pattern made from measured data and that by simulation are most similar to each other, even though a considerable difference was noted between the IP values calculated from the measured data and those from the simulation data.

In this simulation, such data as topography of land surface, shape of IP model, resistivity and FE values, and resistivity of surrounding rock of the IP model were given to a resistor network analog simulator. The results are shown in PL.II-20 (RESULT OF IP MODEL CALCULATION).

The results of simulation are described below.

L-A : The existence of rock bodies with high resistivity is indicated at depths of both ends of the survey line, while low resistivity zone is formed between these high zones. The shape of rock bodies which caused the chargeability anomalies of A and B were assumed as shown in the figure.

L-6 : The shape of rock bodies which caused the chargeability anomalies of C and D were assumed as shown in the figure. It is assumed that the rock which caused C anomaly is surrounded by the rock with high resistivity.

L-8 : Although the profile of measured apparent resistivity along this survey line was very complicated, a pattern was obtained that was similar to the measured profile assuming the structure and resistivity as shown in the figure.

L-11 : The measured profile along this survey line also had a complex shape like that along L-8, and a complex resistivity structure was forecasted. By placing a wide and especially high resistivity model below the center of the survey line, a pattern was obtained that was similar to the measured profile.

L-17 : A structure was presumed as in the figure that caused J-chargeability anomaly.

As mentioned above, since it is theoretically impossible to convert the value itself of time domain method to that of frequency domain method in IP survey or in the simulation, the measured values can not be compared with the calculated values. However, a pattern was obtained that was very similar to the measured profile in the frequency domain IP simulation conducted this time.

Since the maximum resistivity of analog simulator was 6,000 Ω -m, the simulation can not be carried out by using resistivity values larger than this limit. It can be said, however, that the profile obtained as the result of the simulation is quite similar to the measured profile.

6. RESISTIVITY MEASUREMENT OF ROCK SAMPLES

Resistivity of 23 rock samples out of 27 collected in the survey area was measured in the laboratory. Four samples could not be measured because they were broken in sample preparation. For the reference purpose, FE values were measured by a frequency domain method.

The locality of samples is shown in PL.II-21 (INTERPRETATION MAP OF IP SURVEY). The type and the number of rock samples collected are given below, and the results of measurement are shown in Table II-5.

Limestone	2 pcs.
Fine-grained limestone	7 "
Marly limestone	3 "
Recrystallized limestone	15 "
Total	27 "

From the results of measurement, following tendencies are shown.

- (1) The values such as $FE = 1.2 \sim 1.6 \%$ and $\rho_a = 7,000 \sim 18,000 \Omega\text{-m}$ are obtained in many rock samples which contain hematite.
- (2) The values of both FE and ρ_a are large in marly limestone.
- (3) $FE = 0.5 \sim 1.0 \%$ and $\rho_a = 8,000 \sim 20,000$ are shown in many recrystallized limestone samples which do not contain hematite.

Table II-5 Physical properties of rocks (1)

Sample No.	Rock name	Location	Resistivity (Ω -m)	FE (%)	Macroscopic features
22	Limestone	L-16, 500	7,165	1.4	Gray-light reddish brown, calcite-hematite band (w=0.1mm).
23		L-16, 1100	----	--	Gray-light reddish brown, weakly recrystallized?, stylolite-structured, hematite-stained.
1		L- C, 1000	----	--	Gray, fine-grained, weakly recrystallized?, hematite psuedomorph(after pyrite)-spotted.
2		L- A, 1000	20,680	1.0	Gray, fine-grained, very weakly recrystallized?, hematite psuedomorph(after pyrite)-disseminated weakly.
3		L- O, 1100 L- 1, 1100	18,526	0.5	Dark gray, fine-grained, hematite(after pyrite)-disseminated.
5	Fine-grained limestone	L- 3, 1000	1,161	1.6	Reddish brown, fine-grained, hematite psuedomorph(after pyrite)-disseminated.
14		L-11, 900	3,280	0.9	Dark gray, fine-grained, penetrated by calcite veinlets (w=0.5mm).
19		L-14, 400	26,473	0.7	Light brown, fine-grained, weakly recrystallized?.
26		L-18, 700	5,446	0.8	Gray, fine-grained.
4		L- 3, 400	14,430	3.5	Black, fine-grained, marly.
6	Marly limestone	L- 4, 300	19,499	0.6	Black, marly, fine-banded.
24		L-17, 1000	8,130	4.4	Black, fine-grained, marly, banded.
7	Recrystallized limestone	L- 5, 600	19,530	1.0	Reddish pink, weakly recrystallized, hematite (after pyrite)-disseminated.
8		L- 6, 800	----	--	Light gray, weakly recrystallized, hematite (after pyrite)-disseminated.

Physical properties of rocks (2)

Sample No.	Rock name	Location	Resistivity (Ω -m)	FE (%)	Macroscopic features
9		L- 6, 1300	20,372	0.7	Brownish gray, weakly recrystallized, penetrated by hematite-calcite veinlets (w=0.5mm).
10		L- 7, 1100	8,399	0.6	Pinkish, weakly recrystallized, hematite(after pyrite)-disseminated.
11		L- 8, 600	18,327	1.6	Light reddish pink, weakly recrystallized, hematite (after pyrite)-disseminated.
12		L- 8, 1100	16,644	0.5	Grayish white, weakly recrystallized, hematite (after pyrite)-disseminated
13		L- 9, 1200 L-10,	7,885	1.2	Grayish white, weakly recrystallized, stylolite-structured.
15	Recrystallized limestone	L-11, 1250	15,190	1.2	Light brown, recrystallized, hematite-stained along folded bedding planes.
16		L-12, 500	3,240	2.0	Grayish white-light reddish pink, weakly recrystallized, penetrated by calcite veinlets (w=1mm).
17		L-13, 900	20,302	1.2	Grayish white, weakly recrystallized.
18		L-13, 1300	10,614	0.6	Light reddish brown, weakly recrystallized, hematite-stained along bandings.
20		L-14, 1000	----	--	White, weakly recrystallized, hematite (after pyrite)-disseminated.
21		L-15, 1300	13,302	1.0	Light reddish brown, weakly recrystallized, penetrated by calcite veinlets (w=1mm).

Physical properties of rocks (3)

Sample No.	Rock name	Location	Resistivity (Ω -m)	FE (%)	Macroscopic features
25	Recrystallized limestone	L-18, 300	18,032	1.0	Grayish white, weakly recrystallized, penetrated by calcite veinlets (w=0.5mm).
27		L-19, 500	11,469	1.5	Grayish white, weakly recrystallized, penetrated by hematite veinlets (w=1mm).

7. . CONSIDERATION

From the results of the present survey, following conclusions are derived.

- (1) While the chargeability measured in the survey area showed minimum value of 5.5 milli-sec. and maximum value of 55 milli-sec., the values between 5 and 25 milli-sec. were considered to be the background generally endowed with the rocks in the survey area, and the values higher than 25 milli-sec. were taken to be anomaly.
- (2) The values of apparent resistivity measured in the area were distributed in the wide range between 150 and 82,000 Ω -m, and the average of values at all survey points was approximately 5,000 Ω -m. The area is widely underlain by limestones, and the range of measured values described above is considered to be quite common for apparent resistivity of the limestone.
- (3) Seventy percent of the chargeability anomalies designated as A, B, Q were distributed in the zones in which the average value of apparent resistivity was lower than 3,000 Ω -m. It is assumed that these anomalies were caused by fine-grained sulfide minerals in limestone and/or pelitic beds containing carbonaceous matter.
- (4) The magnitude of chargeability anomalies is in the range of 25 ~ 55 milli-sec. These values are by no means the strong chargeability anomaly, being one to two folds of the background values. Judging from the magnitude of anomalous values and the apparent resistivity values of the anomaly zones, the content of sulfide mineral or carbonaceous matter is hardly considered to be abundant. Particularly, it is assumed that sulphide mineral is small in amount.
- (5) It is assumed that the chargeability anomalies distributed in the zone of higher apparent resistivity are associated with ore deposits or mineralized zones. Anomalies such as F, L, and M fall into this category.
- (6) Recrystallized zone of limestone consists the most part of the survey area, and the central part of this zone presents a zone of high resistivity higher than 10,000 Ω -m.

- (7) Most of the chargeability anomalies are distributed along the periphery of the recrystallized zone, while only some small-scale anomalies are found within this zone.
- (8) From the result of measurement on the resistivity and IP of the rock samples, recrystallized limestone which contains hematite tends to have higher values of both resistivity and chargeability.
- (9) By a comprehensive study made on the maps and profiles of chargeability, apparent resistivity and apparent metal factor, IP simulation, and surface geological maps, the result is compiled in PL.II-21 (INTERPRETATION MAP OF IP SURVEY).

PART III

DIAMOND DRILLING

1. GENERAL REMARKS

1.1 Purpose of Diamond Drilling

Diamond drilling of the five drill holes (with a total drilled length of 1,240.90 m) in Table III-1 was performed to shed light on subsurface features of geochemical anomalies, IP anomalies, thermal metamorphic zones and mineralized zones disclosed by the geological and geochemical surveys in Phase III and the geophysical survey and geological survey in the current phase, and thereby examine the possibility of occurrence of ore deposits.

Table III-1 Location, depth and inclination of drill holes

Drill hole	UTM coordinates		Elevation (m)	Depth (m)	Inclination
	E	N			
DDH-M1	647,927	3,124,010	1,565.3	302.25	Vertical
DDH-M2	647,758	3,123,934	1,546.5	302.20	S35°E,-80°
DDH-M3	648,200	3,124,134	1,561.2	212.25	Vertical
DDH-M4	647,493	3,123,160	1,537.5	203.25	Vertical
DDH-M5	647,856	3,123,926	1,553.6	220.95	N55°W,-55°
Total				1,240.90	

1.2 Selection of Drill Sites

The results of the geological and geochemical surveys carried out in Phase II and III as well as the findings of preliminary analysis of the geophysical survey (electric survey of IP method) and geological survey performed prior to the diamond drillings were taken into consideration in selecting the location of the drill holes. The drill holes were selected for the reasons and for the purposes stated below.

DDH-M1

This drill hole was selected because of its location in the southern part of a depressed zone showing a topographical anomaly in the central part

of the area, where a somewhat protruded hill is formed surrounded by strongly recrystallized zones and mineralized zones with green copper indications. The hole was aimed primarily at investigating the geological structure of the depths of the thermal metamorphic zone and the mineralized zone.

DDH-M2

In the vicinity of this drill hole, the geological survey disclosed the presence of garnet veins surrounded by strongly silicified hematite-quartz-calcite veins. For this reason, the zones adjacent to the drill hole were considered to be affected by the most intense thermal metamorphism and hydrothermal alteration in the area. The hole was aimed primarily to investigate the situation of the mineralized zones underlying the thermal metamorphic zones and to examine whether skarnized zones or intrusive igneous rocks occur in the lower part of the thermal metamorphic zones.

DDH-M3

About 300 m east-northeast of the base camp there are found relatively large prospects surrounded by mineralized zone composed of numerous NE-SW trending hematite veins accompanied by green copper indications. In the lower parts of the prospects, the mineralized parts are of manto-type along the bedding planes. In view of this, DDH-M3 was drilled primarily for the purpose of examining whether mineralization had taken place in an extension of the mineralized zone.

DDH-M4

The preliminary analysis of the results of the electric survey of IP method revealed the presence of high-chargeability anomalies at LA-400/1300 and LB-600/1300. This drill hole was conducted to investigate the situation of the deeper part of the high-chargeability anomalies and to ascertain whether the anomalies were related to mineralization.

DDH-M5

This hole was drilled for the primary purpose of determining the dimensions and occurrence of the mineralized zone confirmed by DDH-M2.

The initial planned depth was 300 m for DDH-M1 and 212.5 m for each of DDH-M2, DDH-M3, DDH-M4 and DDH-M5 for a total of 1,150 m. However, the depths were increased or decreased as necessary depending on the geological conditions actually encountered. The final depths drilled are as shown in Table III-1.

1.3 Drilling Method

The area selected for drilling operations is composed primarily of limestone. It was considered likely that diamond drilling operations would encounter skarnized zones and igneous rocks in the depths after drilling the limestone beds characterized by numerous cracks and recrystallization. It was also assumed that the limestone beds and the igneous rocks contained fractured zones and heavily altered zones respectively. Taking these possibilities into account, the wire-line method was adopted which involved the use of drilling mud and diamond bits that would minimize the travelling times of drill pipes and provide greater ease of protection of the hole walls.

At first, drilling mud was used in drilling the DDH-M1, but frequent bonding of the bentonite to the inner face of the drill pipe hampered the passage of the inner tube. For this reason, the use of the drilling mud was discontinued later and it was replaced by fresh water.

In all the drill holes except DDH-M4, heavy lost circulation of drilling water occurred due to a wide distribution of small open fissures in the recrystallized limestone. Cementation was employed to prevent lost circulation of drilling water.

However, a high salt content of the drilling water resulted in a very rapid solidification of the cement, and this gave rise to the possibilities that the pipes might be stuck during cementation in the depths, that during cementation at a normal pressure the cement would fill only wide fissures and that during the reaming of the cement lost circulation would start again after it passed the bottom of the drill hole.

Subsequently, drilling operations were continued without circulating drilling water through the drill holes.

.

However, drilling without circulating water in the drill holes involved a great possibility of occurrence of troubles, such as damage of bits due to the impact produced by the drop of the inner tube and stuck of bits due to the lack of drilling water. Every member of the crews was warned of this possibility, and every care was taken to prevent troubles, but some were unavoidable.

1.4 Personnel and Shift Work

The personnel engaged in the drilling operations consisted of two Japanese and two Mexican drilling engineers and four helpers. One shift worked nine hours during preparation, withdrawal and removal, and two shifts worked eight hours each during drilling. The working time was extended as necessary during the insertion and extraction of casing pipes in order to avoid damage to the hole walls.

Adding to the personnel directly engaged in the drilling operations a man took care of the water pump at Rancho Jabali, a driver and his assistant operated a 10-ton capacity tank lorry and three men took charge of the upkeep of the base camp. In addition, a Japanese and a Mexican geologists stayed there to undertake the selection of drilling sites and identification, description and inspection of drilled cores as well as to prepare for contingencies.

1.5 Drilling Equipments and Consumed Materials

Drilling equipments and consumed materials used in the drilling operations of the present phase were mostly those employed in the preceding phase and later stored in the warehouses owned by the CRM office in Sabinas. HO-WL tools were also supplied to cope with the possible distribution of skarnized zones, fault fracture zones and strongly altered igneous rock bodies in the deeper parts of the survey area and to overcome possible difficulty in obtaining necessary equipments and materials as a result of traffic tieup on the bad roads around the area after heavy rainfall.

Polyethylene water tanks of 3 to 5 m³ in capacity, water pumps and power generator were also provided.

Table III-2 gives details of the equipment procured, all of which was transferred to CRM after the completion of the drilling operations. An adequate quantity of expendable materials, whose breakdown is given in Table III-3 and 4, was also procured in view of the fact that the drilling sites were inconveniently located.

1.6 Identification, Analysis and Storage of Drilled Cores

Cores obtained from the drill holes were brought to the base camp for identification, description and marking for chemical analysis. They were then carried to the CRM office in Sabinas, where after being photographed they were, when necessary, split into halves with a diamond cutter and a core splitter for analysis of four elements, namely, Ag, Cu, Pb and Zn. All the remnant cores were stored in the warehouse of the CRM office.

Of the samples used in the analysis, those separated by method of quartering and weighing about 15 g were transported to Japan for analysis of Au. Samples of relatively high grade were also reanalyzed in Japan for As, Hg, Cd, Co together with Ag, Cu, Pb, Zn. The reanalysis revealed a significant difference in respect of Ag, and in consequence all the core samples were reanalyzed for Ag.

The collected core samples were also used in various tests in Japan such as microscopic observation of thin and polished sections, X-ray diffraction and electron probe microanalysis.

The results of identification and description of the core samples are compiled in the geological corelogs (PL. III-2-1 - 2) together with the results of the various tests conducted.

1.7 Communication

Radio communication was maintained between the CRM office in Sabinas and the base camp for routine contacts or in case of emergencies.

The equipment employed was of the following specifications:



Model	:	IRASA Model "TLALOC" IR-150-3
Output	:	150 W
Frequency available	:	5125, 9886, 14360 KHz
Frequency used	:	5,125 KHz

1.8 Process of Drilling Operations

Table III-5 shows the entire process of drilling operations.

Table III-2 Drilling equipment

Item	Type	Quantity	Specification
Drilling machine	TGM-5A (Tone Boring, Co.)	1 set	Capacity: HQ NQ510m, BQ660m, Inner diameter of spindle: 93mm Spindle speed: 140, 340, 525, 690 r.p.m. Weight (excl. engine) 1,600 kg
Wireline hoist	WHS-600 (Tone Boring, Co.)	1 "	Attached to drilling machine
Engine for drilling machine	F3L-912 (Mitsui Deuts Co.)	1 "	Diesel engine: 4 cycle air-cool type Revolution: 1,800 ~ 1,500 r.p.m. Related power: 40 ~ 33.5 P.S.
Drilling pump	NAS-3B (Tone Boring, Co.)	1 "	Type: 2 cylinders - Double acting Piston diameter: 75mm Capacity: 105 l/min. Pressure: 32 kg/cm ²
Engine for pump	TS-130C (Yammer Diesel Co.)	1 "	Diesel Engine Revolution: 2,200 r.p.m. Related Power: 11 P.S.
Mud mixer	MCE-100A	1 "	Tank Capacity: 125l Effective capacity: 100l Propeller Revolution: 800 ~ 1,000 r.p.m.
Engine for mixer	TS-50	1 "	Diesel Engine Revolution: 2,000 r.p.m. Related power: 4 P.S.
Derrick	DC-P7	1 "	Steel structural derrick (Vertical) Max. load capacity: 6t Effective length of pull rod: 6m
Generator	YSG-2SN	1 "	2KVA 100 ~ 110A
Engine for generator	NS-40	1 "	Diesel engine Revolution: 2,000 r.p.m. Related power: 4 P.S.
Generator	GR-1G	1 "	100V, 1KVA
Water pump	YKC-20	1 "	0.3 m ³ /min.
Engine for pump	NSA-40	1 "	Diesel engine Revolution: 2,000 r.p.m. Related power: 4 P.S.

(continued)

Item	Type	Quantity	Specification
Water tank		7 sets	Plastic tank 5 m ³ : 5 sets 1.5 m ³ : 3 sets
Drill rod	HQ x 3.05m HQ x 1.52 NQ x 3.00 NQ x 3.05 NQ x 1.50 BQ x 3.00 BQ x 3.75 BQ x 1.52 AQ x 3.05	50 pcs 2 " 70 " 20 " 2 " 67 " 33 " 2 " 15 "	
Casing pipe	HW x 1.52 HW x 0.61 NW x 3.00 NW x 3.05 NW x 1.00 BW x 3.00 BW x 3.05 BW x 1.00	20 pcs 20 " 10 " 45 " 2 " 43 " 46 " 2 "	
Wire line core barrel	HQ x 3.05m NQ x 3.00 NQ x 3.05 BQ x 3.00 BQ x 3.05	3 sets 3 " 1 " 3 " 1 "	
Single core tube	114mm x 1.50m 114mm x 0.50 99mm x 1.50 99mm x 0.50	1 set 1 " 1 " 2 "	
Water swivel	EH	1 set	
Hoisting swivel	B	1 set	
Rod holder	RH-85 E-7454	1 set 1 "	
Inclinater	Tro-pari	1 "	

Table III-4 Specifications of metal crown, diamond bits, reaming shells and casing shoe bits

Item	Type	Carats per bit	Matrix	Carats per stone	Water way	Bit No.	Remarks
Metal crown	Single crown						115 mm
Diamond bit	NQ-WL	30 ct	T1	1/20~1/35 ct	4	T-474	
		"	"	"	"	T-476	
		"	"	"	"	T-751	
		"	"	"	"	T-754	
		"	Z	1/25~1/30	"	E-3810	
		"	Z	"	"	E-3814	
Diamond reaming shell	NQ-WL-R	6.6	T1	1/20~1/35	4	TR-490	
		"	"	"	"	TR-491	
		8	ZZ	1/25~1/30	"	EG-3835	
Diamond bit	BQ-WL	20	T1	1/20~1/35	4	T-757	
		"	A	1/15~1/40	"	T-73873	
		"	"	"	"	T-73878	
Diamond reaming shell	BQ-WL-R	6	(Z)	1/25~1/30	4	BRAN-574	
Casing shoe bit	NW		T1	1/20~1/35	4	T-773	

Table III-5 Progress of drilling works

Item	Jul.	Aug.	Sep.	Oct.	Nov.	Remarks
1 Trip (Japan-drilling site)	14-19					
Preparation of camp						
2 Construction of access road (by C.R.M.)	20-25					
Haulage, Preparation	25	14				
DDH-N1						
Drilling		15				
Dismounting		16-18				
Haulage, Preparation						
DDH-N2						
Drilling		19	8			
Dismounting			9			
Haulage, Preparation			10-11			
DDH-N3						
Drilling			12-24			
Dismounting			25			
Haulage, Preparation			26-27			
DDH-N4						
Drilling			28-30			
Dismounting			31			
Haulage, Preparation						
DDH-N5						
Drilling				6-7		
Dismounting				8-15		
Haulage (Drilling site-Base Camp)				16-19		
4						
5 Trip (Drilling site-Japan)				20-22		
6 Inspection of core and others						

2. DRILLING OPERATION

2.1 Arrangement

2.1.1 Preparation

Mina la Diana and its surroundings where the drilling operations were conducted in the present phase are located in a private-owned pasture ground, and the road conditions were extremely bad. Since water was not available in the neighborhood of the drilling sites, all drilling water had to be obtained from Rancho Jabali about 10 Km distant. Before the drilling operations, the existing road linking the drilling sites with Rancho Jabali was improved, and a new road was constructed across the survey area. In addition, a wooden house having a floor space of 50 m² was built to accommodate more than 10 persons.

These preparations were made by the CRM officials in Sabinas at the request of the survey team. A bulldozer was the primary equipment employed in the improvement and construction of the roads. Explosives were also used where limestones cropped out. The total length of roads constructed and improved in 11.0 Km, of which 4.0 Km represents the new road and 7.0 Km the existing road repaired.

HQ-WL tools and expendable items such as oil and gasoline were procured in Mexico City, Sabinas and adjacent areas, and stored in CRM's warehouses in Sabinas.

2.1.2 Transportation of Equipments and Materials to the Drilling Site

Two Japanese drilling engineers arrived in Mexico City on July 14 and after a round of courtesy calls at Government agencies concerned, they departed for Sabinas where they inspected and serviced drilling equipments stored at CRM's warehouses as well as newly procured equipments and materials.

These equipments and expendable materials were transported to the drilling site (DDH-M1) by a truck of 10-ton capacity between July 17 and 24. After installation and test run of the drilling machine and other equipment, the drilling work was started on July 26.

2.2 Removal of Drilling Equipment

Roads for the transportation of drilling equipment between drilling sites were relatively short and were constructed primarily with human power in a period of one or two days. The new roads for the drill holes are as listed below:

- DDH-M1 : On road side; no need for new road construction
- DDH-M2 : On road side; no need for new road construction
- DDH-M3 : About 100 m distant from existing road; new road completed with human power in a single day.
- DDH-M4 : About 50 m distant from existing road; new road completed with human power in a single day.
- DDH-M5 : About 70 m distant from existing road; new road completed with human power in two days.

A 10-ton truck was used to haul drilling equipment between drilling sites. The haulage was completed in a single day for each drill hole, as the distances between drill holes were short and haul roads had been constructed.

2.3 Withdrawal

Drilling operation was started on July 24, made a rather smooth progress, and was brought to total completion on October 19, in spite of some troubles such as inner tube damage in DDH-M2 and drill pipe stuck in DDH-M3. These troubles could be overcome without much difficulty thanks to adequate replacements and appropriate measures. Anticipated conspicuous skarn zones, fracture zones accompanied by caving or heavily altered igneous rock bodies were not encountered.

After the completion of the operation, the drilling equipment was dismounted and brought to the base camp together with the unused expendable items after a thoroughgoing inspection and servicing. All the equipment and unused materials were transferred to CRM together with their list. Table III-6 gives a breakdown of the days required for removal and withdrawal.

Table III-6 Moving operations

Item	Drilled hole No.		DDH-M1		DDH-M2		DDH-M3		DDH-M4		DDH-M5		Total	
	Days	Man shift	Days	Man shift	Days	Man shift	Days	Man shift	Days	Man shift	Days	Man shift	Days	Man shift
Moving operation	Preparation		20th Jul. '78	16th Aug. '78	10th Sep. '78	26th Sep. '78	6th Oct. '78							
	Dismounting		25th Jul. '78	18th Aug. '78	11th Sep. '78	27th Sep. '78	7th Oct. '78							
			15th Aug. '78	9th Sep. '78	25th Sep. '78	4th Oct. '78	16th Oct. '78							
			"	"	"	"	5th Oct. '78	19th Oct. '78						
Preparation	Unpacking, etc.		1	8									1	8
	Checking, loading		2	6									2	6
	Haulage		1	4										
	Unloading, site-leveling, machine bed installation		1	9	2	22	1	8	1	8	1	8	7	59
	Machine fabrication													
	Derrick fabrication													
	Test operation		1	30	1	14	1	8	1	8	1	8	5	68
	Drilling preparation													
	Total		6	57	3	36	2	16	2	16	2	16	15	141
	Dismounting	Pulling out of casing pipe		1	10	0.5	4	0.5	4	2	18	1	9	6
Dismounting				0.5	7	0.5	5							
Haulage, etc.												3	21	
Total		1	10	1	11	1	9	2	18	4	30	9	78	

2.4 Core Recovery and Protection of Hole Walls

The survey area is located in a mountainous part composed mainly of limestone, where the soil layer has a rather limited thickness, and below the soil layer is hardly formed weathered bedrocks. At DDH-M1 and DDH-M2, limestone outcrops were observed. In DDH-M4, the soil layer was thickest as 5.9 m. Soil layers were drilled without water by means of a 115 mm single core tube with a metal crown, and when the bedrock was reached HW casing pipes were inserted, and drilling was performed with NQ-WL diamond bit using fresh water.

Fractured and fragmentarily brecciated part are found in limestone beds frequently, however, those were mostly filled with calcite, and they were not easy to cave in. In some heavily fractured zones circulation of mud water or injection of cement milk was used, but these measures were discontinued for the reasons previously mentioned, and casing pipes were inserted into drill holes to protect their walls. In these fracture zones, the drilling length of a run was shortened to improve core recovery, and satisfactory results were generally obtained. Table III-7 gives core recovery in percentage for the five drill holes. In no case did the core recovery at every 50 m of drilling show less than 80%.

Table III-7 Core recovery of each hole

Drill hole	Depth (m)	Core length (m)	Core recovery (%)
DDH-M1	302.25	288.69	95.51
DDH-M2	302.20	277.90	91.96
DDH-M3	212.25	206.40	97.2
DDH-M4	203.25	203.15	99.9
DDH-M5	220.95	208.45	94.3
Total	1,240.90	1,184.59	95.46

Casing pipes were used only when the drill hole was likely to cave in and NQ-WL bits were employed wherever possible.

Table III-8 Drilling condition and result at each hole

Depth	DDH-M1		DDH-M2		DDH-M3		DDH-M4		DDH-M5	
	0~260.25m	260.25 ~302.25m	0~133.15m	133.15 ~302.20m	0~155.80m	155.80 ~212.25m	0~203.25m	203.25 ~220.95m	0~220.95m	220.95 ~240.00m
Circulating water	Clean water	Clean water	Clean water	Clean water	Clean water	Clean water	Clean water	Clean water	Clean water	Clean water
Bit change	NQ-WL diamond bit 3 times	BQ-WL diamond bit 1 time	NQ-WL diamond bit 2 times	BQ-WL diamond bit 3 times	NQ-WL diamond bit 1 time	HW diamond bit 1 time	NQ-WL diamond bit 1 time	NQ-WL diamond bit 1 time	NQ-WL diamond bit 1 time	NQ-WL diamond bit 1 time
Pump	Pressure(kg/cm ²)	2	1	1	1	1	1	1	1	2
	Feed water (ℓ/min)	40	40	40	40	40	40	40	40	40
	Return water (%/min)	0	0	0	0	0	0	0	0	0
Bit	Pressure(kg/cm ²)	200~500	500	500	500~100	1,000~500	1,000~500	500~1,000	1,000	1,000
	Revolution (r.p.m.)	250	250	250	250	250	250	250~450	450	450
Core recovery (%)	95.08	98.21	89.82	93.64	97.6	-	99.95	96.3	99.95	94.34

Table 111-9 Drilling length by metal crown, diamond bit, reaming shell and casing shoe bit

Item	Size	Type	Bit No.	DDH-W1		DDH-W2		DDH-W3		DDH-W4		DDH-W5		Total length	Remarks
				depth	length	depth	length	depth	length	depth	length	depth	length		
Metal crown	115 m/s	Single crown		0-2.25	2.25	0-0.60	0.60	0-5.80	5.80	0-5.90	5.90	0-1.90	1.90	2.25 0.60 5.80 5.90 1.90	
Total				2.25	2.25	0.60	0.60	5.80	5.80	5.90	5.90	1.90	1.90	16.45	
Diamond bit	NQ	NQ-WL	T-476	2.25 16.00 218.25	13.75 202.25	0.60 35.00 130.15	34.40 95.15	5.80 131.60 112.25	125.80 80.65	5.90 203.25				13.75 202.25 76.40 220.95 278.00	
Total				258.00	258.00	129.55	206.45	206.45	206.45	197.35	197.35	219.05 220.95	219.05	219.05 1,010.40	
Diamond reaming shell	NQ	NQ-WL-R	TR-491	2.25 260.25	258.00 258.00	0.60 35.00 130.15	34.40	5.80 217.25	206.45	5.90 203.25				292.40 487.95	
Total				258.00	258.00	129.55	206.45	206.45	206.45	199.35	199.35	219.05 220.95	219.05	219.05 1,010.40	
Diamond bit	BQ	BQ-WL	T-73873	260.25 302.25	42.00	130.15 231.90 271.40	101.75	39.50	30.80	172.05				143.75 39.50 30.80	
Total				42.00	42.00	172.05	172.05	172.05	172.05	172.05	172.05	172.05	172.05	214.05	
Diamond reaming shell	BQ	BQ-WL-R	BRAM-574	260.25 302.25	42.00	130.15 231.90 271.40	101.75	39.50	30.80	172.05				214.05	
Total				42.00	42.00	172.05	172.05	172.05	172.05	172.05	172.05	172.05	172.05	214.05	
Metal crown	Total		5 pr 4	2.25	2.25	0.60	0.60	5.80	5.80	5.90	5.90	1.90	1.90	16.45	
Diamond bit	Total		9 "	300.00	300.00	301.60	301.60	206.45	206.45	197.35	197.35	219.05	219.05	1,226.45	
Diamond reaming shell	Total		4 "	300.00	300.00	301.60	301.60	206.45	206.45	197.35	197.35	219.05	219.05	1,226.45	
Casing shoe bit	NW		T-773			5.80 153.70	147.50	147.50	147.50					147.50	Reaming

Table III-10 Working time of each drill hole

Drilled hole	Drilling						Sub total	Others	Moving operation	Total
	Drilling time	Hoisting & lowering rod, casing	Repairing	Hoisting & lowering rod, casing	Repairing	Sub total				
DDH-M1	95 ^h 30 ^m	33 ^h 30 ^m	55 ^h 00 ^m	-	184 ^h 00 ^m	36 ^h 00 ^m	65 ^h 00 ^m	285 ^h 00 ^m		
DDH-M2	93 ^h 30 ^m	59 ^h 00 ^m	29 ^h 30 ^m	3 ^h 00 ^m	185 ^h 00 ^m	8 ^h 00 ^m	34 ^h 00 ^m	227 ^h 00 ^m		
DDH-M3	68 ^h 30 ^m	30 ^h 00 ^m	23 ^h 30 ^m	71 ^h 00 ^m	193 ^h 00 ^m	-	27 ^h 00 ^m	220 ^h 00 ^m		
DDH-M4	52 ^h 30 ^m	16 ^h 30 ^m	15 ^h 00 ^m	-	84 ^h 00 ^m	-	34 ^h 00 ^m	118 ^h 00 ^m		
DDH-M5	72 ^h 00 ^m	26 ^h 00 ^m	26 ^h 00 ^m	-	124 ^h 00 ^m	-	48 ^h 00 ^m	172 ^h 00 ^m		
Total	382 ^h 00 ^m	165 ^h 00 ^m	149 ^h 00 ^m	74 ^h 00 ^m	770 ^h 00 ^m	44 ^h 00 ^m	208 ^h 00 ^m	1,022 ^h 00 ^m		

Table III-11 Results of drilling works

Drilled hole No.	Machine type	Drilling period	Drilled depth (m)	Core		Number of drilling shift			Drilling speed		Remarks
				Length (m)	Recovery (%)	No. of drilling	Casing, etc.	Shift total	* M/shift	** M/shift	
DDH-M1	TGM-5A	26th Jul. '78 ~14th Aug. '78	302.25	288.69	95.51	20	1	21	15.11	14.39	
DDH-M2	"	19th Aug. '78 ~8th Sep. '78	302.20	277.90	91.96	19	1	20	15.91	15.11	
DDH-M3	"	12th Sep. '78 ~24th Sep. '78	212.25	206.40	97.24	16	8	24	13.27	8.84	
DDH-M4	"	28th Sep. '78 ~3rd Oct. '78	203.25	203.15	99.95	10	0	10	20.33	20.33	
DDH-M5	"	8th Oct. '78 ~15th Oct. '78	220.95	208.45	94.34	15	0	15	14.73	14.73	
Total	"	20th Jul. '78 ~19th Oct. '78	1,240.90	1,189.24	95.84	79	10	89	15.71	13.94	

Note: * Drilled length per one shift covering net drilling operations.

** Drilled length per one shift covering total works conducted.

Table III-12 Summary of drilling results: DDH-M1

Item	Working period		Number of days	Actual working days	Repairing days	Road re-pairing days	Total number of workers		
							excl. Road repairs	incl. Road repairs	
Preparation	20th Jul.'78~25th Jul.'78		6	6	0	0	57	57	
Drilling	26th Jul.'78~14th Aug.'78		20	16	0	4	155	246	
Dismounting	15th Aug.'78		1	1	0	0	10	10	
Total	24th Jul.'78~15th Aug.'78		27	23	0	0	214	305	
Drilling length, etc.			Core recovery for each 100m section						
Planned length	300.0 m	Over-burden	0 m	Depth of hole		Section	Total		
Increase or decrease in length	+2.25 m	Core length	288.69m	0~100.05 m		96.69 %	96.69 %		
				100.05~200.50 m		97.07 %	96.88 %		
Length drilled	302.25 m	Core recovery	95.51%	200.50~302.25 m		93.32 %	95.51 %		
Working time	Drilling	Drilling	95 ^h 30 ^m	51.9 %	33.5 %	Drilling efficiency			
		Hoisting & lowering rod, casing	33 ^h 30 ^m	18.2 %	11.8 %	302.25 m/Working period		11.19 m/day	
		Repairing	-	- %	- %	302.25 m/Working days		13.14 m/day	
		Others	55 ^h 00 ^m	29.9 %	19.3 %	302.25 m/Drilling period		15.11 m/day	
		Sub total	184 ^h 00 ^m	100.0 %	64.6 %	302.25 m/Net drilling days		18.89 m/day	
	Preparation	57 ^h 00 ^m		20.0 %	Total workers/302.25 m (incl. Road repairs)		1.01 man/m		
	Dismounting	8 ^h 00 ^m		2.8 %					
	Others *	36 ^h 00 ^m		12.6 %	Total workers/302.25 m (excl. Road repairs)		0.71 man/m		
	Total	285 ^h 00 ^m		100.0 %					
	Inserting casing pipe	Pipe size & inserted length (m)	Inserted length / Drilling length x 100%	Recovery of casing pipe (%)	Total drilling workers/302.25m (incl. Road repairs)		0.81 man/m		
HW.C.P.: 2.25		0.7	100	Total drilling workers/302.25m (excl. Road repairs)		0.51 man/m			
BW.C.P.: 260.25		86.1	100	Drilling length by each size (m)					
				Bit size	115 mm	NQ	BQ		
				Drilling length	2.25	258.00	42.00		
			Core length	1.65	245.79	41.25			
Remarks: * Waiting for water and road repairing.									

Table III-13 Summary of drilling results: DDH-M2

Item	Working period		Number of days	Actual working days	Repairing days	No working days	Total number of workers	
Preparation	16th Aug.'78~18th Aug.'78		3	3	0	0	36	
Drilling	19th Aug.'78~ 8th Sep.'78		21	17	0	4*	146	
Dismounting	9th Sep.'78		1	1	0	0	11	
Total	16th Aug.'78~ 9th Sep.'78		25	21	0	4	193	
Drilling length, etc.				Core recovery for each 100m section				
Planned length	212.5 m	Over-burden	0 m	Depth of hole	Section	Total		
Increase or decrease in length	+89.7 m	Core length	277.90m	0~100.25 m	96.36 %	96.36 %		
				100.25~200.95 m	86.84 %	91.59 %		
Length drilled	302.20 m	Core recovery	91.96%	200.95~302.20 m	92.69 %	91.96 %		
Working time	Drilling	Drilling	93 ^h 30 ^m	50.5 %	41.2 %	Drilling efficiency		
		Hoisting & lowering rod, casing	59 ^h 00 ^m	31.9 %	26.0 %	302.20 m/Working period		12.09 m/day
		Repairing	3 ^h 00 ^m	1.6 %	1.3 %	302.20 m/Working days		14.39 m/day
		Others	29 ^h 30 ^m	16.0 %	13.0 %	302.20 m/Drilling period		14.39 m/day
		Sub total	185 ^h 00 ^m	100.0 %	81.5 %	302.20 m/Net drilling days		17.78 m/day
	Preparation	25 ^h 00 ^m	/	11.0 %	Total workers/302.20 m		0.64 man/m	
	Dismounting	9 ^h 00 ^m		4.0 %				
	Others	8 ^h 00 ^m		3.5 %	Total workers/		m	
	Total	227 ^h 00 ^m		100.0 %	(excl. Road Repairs)		man/m	
	Inserting casing pipe	Pipe size & inserted length (m)	Inserted length / Drilling length x 100%	Recovery of casing pipe (%)	Total drilling workers/302.20m		0.48 man/m	
HW.C.P.: 0.6		0.2	100	Total drilling workers/		m		
BW.C.P.: 130.15		43	100	Drilling length by each size (m)				
				Bit size	115 mm	NQ	BQ	
				Drilling length	0.6	132.55	169.05	
				Core length	0.6	119.00	158.30	
Remarks: * Waiting for decision of increase in drilling length.								

Table III-14 Summary of drilling results: DDH-M3

Item	Working period		Number of days	Actual working days	Repairing days	No working days	Total number of workers	
							excl. Repairs	incl. Repairs
Preparation	10th Sep. '78~11th Sep. '78		2	2	0	0	16	16
Drilling	12th Sep. '78~24th Sep. '78		13	9	4	0	77	112
Dismounting	25th Sep. '78		1	1	0	0	9	9
Total	10th Sep. '78~25th Sep. '78		16	12	4	0	102	137
Drilling length, etc.			Core recovery for each 100m section					
Planned length	212.5 m	Overburden	5.5m	Depth of hole	Section	Total		
Increase or decrease in length	-0.25 m	Core length	206.40m	0~109.95 m	97.0 %	97.0 %		
Length drilled	212.25 m	Core recovery	97.24%	109.95~212.25 m	97.6 %	97.2 %		
Working time	Drilling	Drilling	68 ^h 30 ^m	35.5 %	31.1 %	Drilling efficiency		
		Hoisting & lowering rod, casing	30 ^h 00 ^m	15.6 %	31.6 %	212.25 m/Working period		13.27 m/day
		Repairing	71 ^h 00 ^m	36.8 %	32.3 %	212.25 m/Working days		17.69 m/day
		Others	23 ^h 30 ^m	12.1 %	10.7 %	212.25 m/Drilling period		16.33 m/day
		Sub total	193 ^h 00 ^m	100.0 %	87.7 %	212.25 m/Net drilling days		23.58 m/day
	Preparation	18 ^h 00 ^m	/	8.2 %	Total workers/ 212.25 m (incl. Repairs)		0.65 man/m	
	Dismounting	9 ^h 00 ^m		4.1 %	Total workers/ 212.25 m (excl. Repairs)		0.48 man/m	
	Others			%				
	Total	220 ^h 00 ^m		100.0 %				
	Inserting casing pipe	Pipe size & inserted length (m)	Inserted length / Drilling length x 100%	Recovery of casing pipe (%)	Total drilling workers/212.25 m (incl. Repairs)		0.53 man/m	
HW.C.P.: 5.80		2.7	100	Total drilling workers/212.25 m (excl. Repairs)		0.36 man/m		
NW.C.P.: 153.30		72.0	100	Drilling length by each size (m)				
				Bit size	115 mm	NQ		
				Drilling length	5.80 m	206.45 m		
				Core length	5.80 m	200.60 m		
Remarks:								

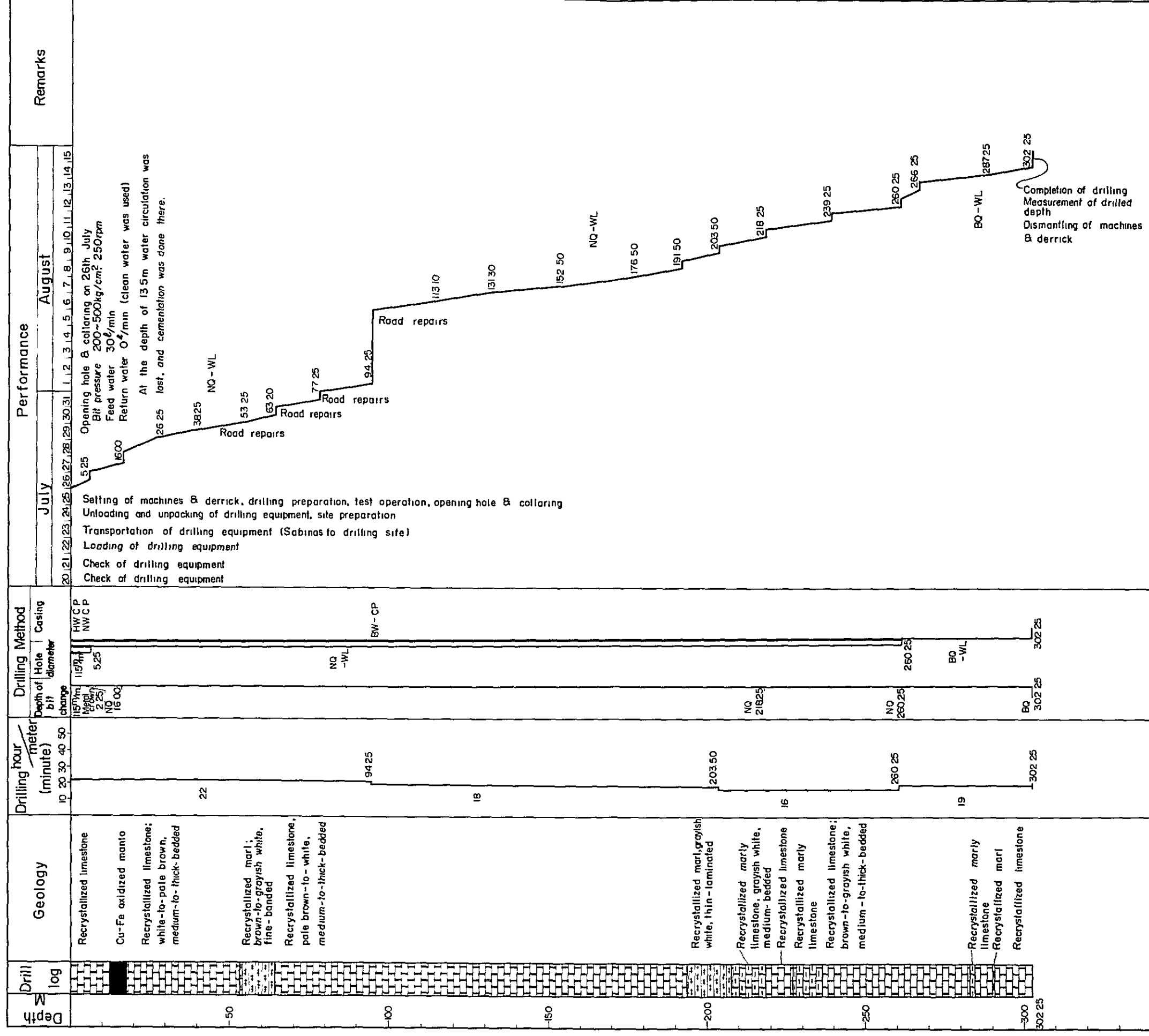
Table III-15 Summary of drilling results: DDH-M4

Item	Working period		Number of days	Actual working days	Repairing days	No working days	Total number of workers	
Preparation	26th Sep.'78~27th Sep.'78		2	2	0	0	16	
Drilling	28th Sep.'78~ 3rd Oct.'78		6	6	0	0	52	
Dismounting	4th Oct.'78~ 5th Oct.'78		2	2	0	0	18	
Total	26th Sep.'78~ 5th Oct.'78		10	10	0	0	86	
Drilling length, etc.				Core recovery for each 100m section				
Planned length	212.5 m	Over-burden	5.90m	Depth of hole	Section	Total		
Increase or decrease in length	-9.25 m	Core length	203.15m	0~106.55 m	99.9 %	99.9 %		
Length drilled	203.25 m	Core recovery	99.95%	106.55~203.25 m	100.0 %	99.9 %		
Working time	Drilling	Drilling	52 ^{h30m}	62.5 %	44.5 %	Drilling efficiency		
		Hoisting & lowering rod, casing	16 ^{h30m}	19.6 %	14.0 %	203.25 m/Working period		20.33 m/day
		Repairing	-	-	-	203.25 m/Working days		20.33 m/day
		Others	15 ^{h00m}	17.9 %	12.7 %	203.25 m/Drilling period		33.88 m/day
		Sub total	84 ^{h00m}	100.0 %	71.2 %	203.25 m/Net drilling days		33.88 m/day
	Preparation	18 ^{h00m}	/	15.3 %	Total workers/203.25 m		0.42 man/m	
	Dismounting	16 ^{h00m}	/	13.5 %				
	Others	-	/	%	Total workers/ m			
	Total	118 ^{h00m}	/	100.0 %	Total workers/ (excl. Repairs) m		man/m	
	Inserting casing pipe	Pipe size & inserted length (m)	Inserted length / Drilling length x 100%	Recovery of casing pipe (%)	Total drilling workers/203.25 m		0.26 man/m	
NW.C.P.: 5.90		2.9	100	Total drilling workers/ m		man/m		
Drilling length by each size (m)								
Bit size		115 mm		NQ				
Drilling length		5.90 m		197.35 m				
Core length		5.90 m		197.25 m				
Remarks:								

Table III-16 Summary of drilling results: DDH-M5

Item	Working period			Number of days	Actual working days	Repairing days	No working days	Total number of workers
Preparation	6th Oct.'78~ 7th Oct.'78			2	2	0	0	16
Drilling	8th Oct.'78~15th Oct.'78			8	8	0	0	72
Dismounting	16th Oct.'78~19th Oct.'78			4	4	0	0	30
Total	6th Oct.'78~19th Oct.'78			14	14	0	0	118
Drilling length, etc.				Core recovery for each 100m section				
Planned length	212.5 m	Over-burden	1.90m	Depth of hole	Section	Total		
Increase or decrease in length	+17.5 m	Core length	208.45m	0~105.75 m	97.0 %	97.0 %		
Length drilled	220.95m	Core recovery	94.34%	105.75~220.95 m	91.9 %	94.3 %		
Working time	Drilling	Drilling	72 ^h 00 ^m	52.0%	41.9 %	Drilling efficiency		
		Hoisting & lowering rod, casing	26 ^h 00 ^m	21.0%	15.1 %	220.95 m/Working period		20.09 m/day
		Repairing	-	-	-	220.95 m/Working days		20.09 m/day
		Others	26 ^h 00 ^m	21.0%	15.1 %	220.95 m/Drilling period		27.62 m/day
		Sub total	124 ^h 00 ^m	100.0%	72.1 %	220.95 m/Net drilling days		27.62 m/day
	Preparation	19 ^h 00 ^m	/	11.0 %	Total workers/ 220.95m		0.53 man/m	
	Dismounting	29 ^h 00 ^m		16.9 %				
	Others	-		- %				
	Total	172 ^h 00 ^m		100.0 %	Total workers/ (excl. Repairs)			man/m
	Inserting casing pipe	Pipe size & inserted length (m)	Inserted length / Drilling length x 100%	Recovery of casing pipe (%)	Total drilling workers/220.95m		0.33 man/m	
115mm C.P.: 1.90		0.9	100	Total drilling workers/ (excl. Repairs)		man/m		
Drilling length by each size (m)								
Bit size				115 mm	NQ			
Drilling length				1.90 m	219.05 m			
Core length			1.90 m	206.55 m				
Remarks:								

Fig. III - 1 Progress Record of Diamond Drilling DDH - M I Vertical



2.5 Procurement of Drilling Water

As mentioned earlier, drilling water had to be transported from Rancho Jabali at some distance from the drilling sites. Since drilling water was completely lost and cementation did not work in all the drill holes except DDH-M4, the drilling operations had to be performed without circulating water through the drill holes. Thus it was an important problem how to obtain drilling water. As a solution for this problem, five 5-ton polyethylene water tanks were installed at each drill hole site to store water brought by a tank lorry to be used in drilling. Water was trucked three to four times a day in normal times. During the drilling of DDH-M1, water supply was stopped for four days because of damage of the haul road due to a heavy rainfall, and all the field personnel had to engage in repairs of the damaged section of the road. In the case of DDH-M2 and three other successive drill holes, the weather and road conditions improved and water supply continued smoothly.

2.6 Drilling Operation

Drilling operations for the five drill holes are described in 2.6.1, to 2.6.5. Table III-8 shows drilling conditions for individual drill holes, Table III-9 results of bits and reaming shells, Table III-10 working hours for the holes, Table III-11 actual performance of the drilling work, Tables III-12 to III-16 summary of the work for each hole, and Figs. III-1 to III-5 progress record of the work for each hole.

2.6.1 DDH-M1 (Depth : 302.25 m, Vertical)

Depth range : 0.00 - 164.50 m

Because of an outcrop of rather weathered recrystallized limestone on the surface, the hole was drilled with a 115 mm metal crown to a depth of 2.25 m. After inserting 115 mm casing pipes, the drilling continued using NQ-WL diamond bits and NW casing pipes was inserted to a depth of 5.25 m.

In the depth ranges of 12.05 to 16.65 m and 16.95 to 17.55 m, silicified iron oxide ores composed mainly of hematite with green copper indications

were encountered. In the depth range of 26.25 to 27.75 m were encountered fragile oxidized iron ores composed primarily of limonite. In this part, cores were collected from a shorter section in an effort to improve the core recovery, but a slight reduction in the core recovery was unavoidable. Other sections consisted partly of saccharoidal recrystallized limestone with marl with numerous fissures which were mostly filled with dogtooth calcite veins. The drilling operations was generally successful, though caving sometimes occurred.

[Use of drilling mud]

At first, bentonite mud water was used when caving took place at a depth of 5.60 m. When drilling went on for about 15 minutes, however, mud stuck to the inner face of the drill pipes, and hindered the passage of the inner tubes. For this reason, the use of the mud water was discontinued forthwith. The trouble was presumably due to the coagulation and precipitation of bentonite caused by the very hard drilling water. Dispersing agent was not available.

[Control of lost circulation]

Complete loss of the circulating drilling water occurred at a depth of 13.50 m. Examination of the core samples recovered disclosed the leaks had taken place in druses and fissures in the mineralized zones. Cementation was applied to stop the leakage, but the solidifying time of cement was considered very short due to the drilling water being very hard. Therefore, there was every possibility of the drill pipes being stuck by the cement when injected in the deeper parts. It was also feared that under the normal pressure the cement might not fill fissures adequately and that loss of water might start again after passing the hole bottom. Further, the reaming of the cement would take too much time due to its rapid solidification. For these reasons, the drilling operation was then performed without circulating water. As a result, however, the drill pipes vibrated heavily during the drilling, and the work was continued pouring 10 liters of water per minute between

the drill pipe and the wall of the hole. This brought about inevitably some reduction in the operation efficiency.

Depth range : 164.50 - 191.50 m

This section consisted largely of saccharoidal recrystallized limestone beds which were heavily fractured and characterized by numerous small fissures and a strong brecciation. However, these fissures were completely filled with dogtooth calcite veins and the drilling made a smooth progress on the whole, though some troubles, such as clogging of core samples, occurred in some parts of the drill hole.

Depth range : 191.50 - 260.20 m

This section consisted of saccharoidal limestone beds intercalated locally with marl beds and oxidized argillaceous beds. Open fissures stained with brown to black iron oxide have a local distribution. They were noticeable especially in the depth range of 209.25 to 218.25 m. Since the clogging of core occurred very frequently, the inner tubes were pulled out frequently so as to achieve improved core recovery. In the depth range of 236.25 to 260.25 m were found fracture zones filled with dogtooth calcite veins. Open fissures have a localized distribution in the fracture zones. This was responsible for a slight reduction in the operating efficiency, but the drilling work progressed smoothly on the whole.

[Insertion of BW casing pipe]

A fall in the operating efficiency as a result of drill pipe vibration became increasingly noticeable with increasing depth. Moreover, some fracture zones were encountered during the drilling and open fissures had a localized distribution in the zones. For all these reasons, there was every possibility of caving. BW casing pipes were inserted into the drill hole when it reached a depth of 260.25 m, in order to protect its walls. Despite the possibility of caving of the drill hole due to vibration of drill pipes, they could be pulled out without being stuck and the casing pipes were inserted without difficulty. The whole work was completed in a single day.

Depth range : 260.25 - 302.20 m

This section was composed mainly of saccharoidal recrystallized limestone beds intercalated locally with marl beds and oxidized thin argillaceous beds. It is characterized on the whole by a wide distribution of fissures and brecciated zones. These fissures were filled thoroughly with dogtooth calcite and this facilitated the drilling operation. At the depth of 300 m, no effect of mineralization was observed, and when the geologists examined the cores obtained, they concluded that the object of the drilling had been attained. Therefore, the operation was stopped after recovering and inspecting the drill pipes and the core length.

2.6.2 DDH-M2 (Depth : 302.20 m, Direction : S35°E, -80°)

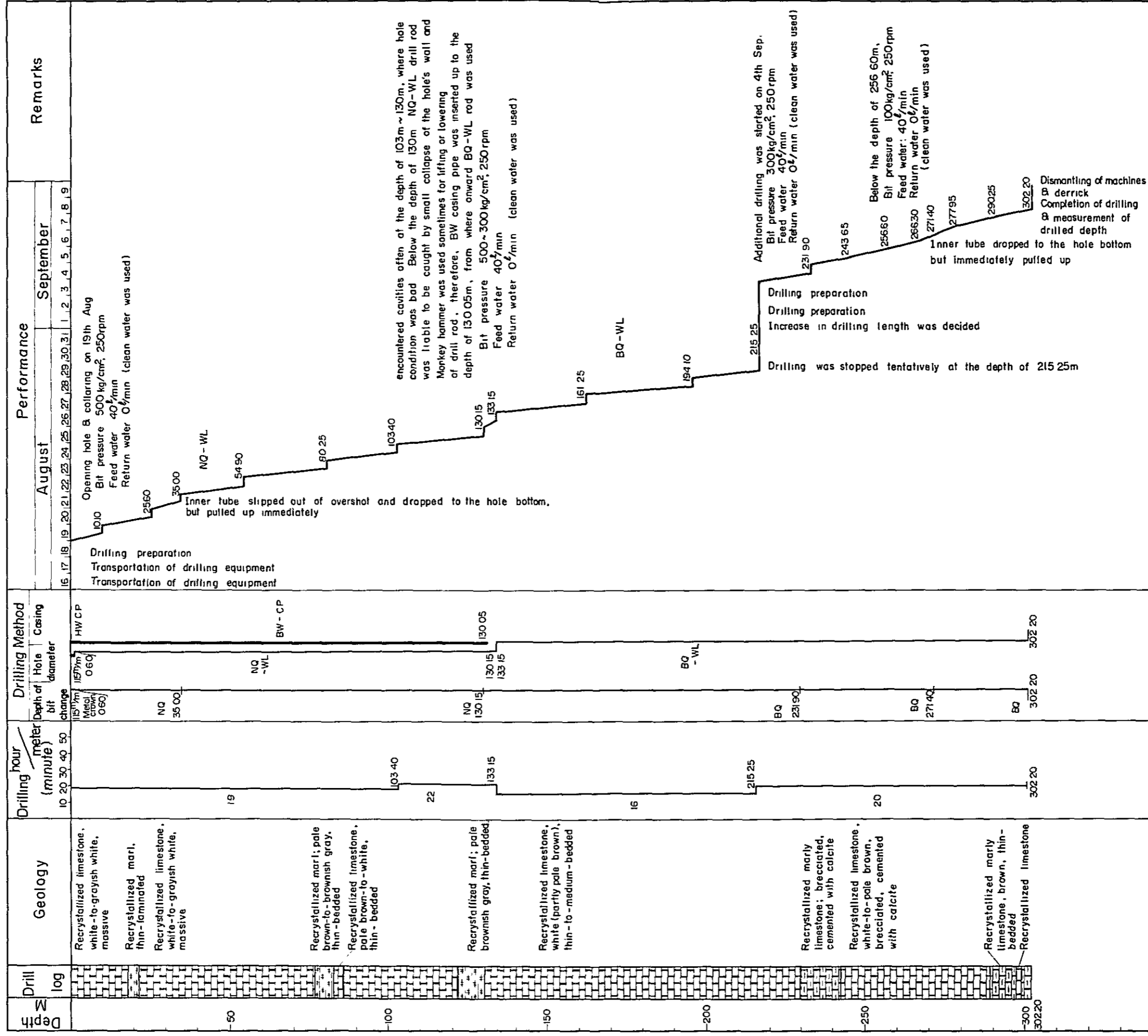
Depth range : 0.00 - 133.5 m

Because of an outcrop of slightly weathered saccharoidal recrystallized limestone at the surface, the hole was drilled with a 115 m metal crown to a depth of 0.60 m. 115 mm casing pipes were then inserted into the hole and the drilling was continued with NQ-WL diamond bits. After reaching a depth of 3.50 m, drilling water was lost completely, however, the drilling was continued without water circulation and pouring about 10 liters of water per minute between the drill pipe and the wall as a precaution against pipe vibration and paying attention to possible washout of sludge.

The geology of this section consists of saccharoidal recrystallized limestone interbedded locally with marl. It is characterized by a general distribution of dogtooth calcite veins. Also found in the section were brecciated zones, thick calcite veins, open fissures and oxidized ore veins. The thick calcite veins occurred in the depth range of 48.35 to 52.20 m with dip ranging from 60 to 85°.

They are porous veins containing numerous druses with similar dips. Major open fissures were found in the depth ranges of 35.70 to 38.15 m, 40.25 to 41.00 m, 70.80 to 77.25 m, 82.40 to 83.85 m, 95.50 to 96.25 m, 103.40 to 105.25 m, 108.30 to 116.60 m and 121.60 to 128.50 m. Cores were often fragmental and stained on the surface with limonite. Like

Fig. III-2 Progress Record of Diamond Drilling DDH-M2 -80°



oxidized ore veins, the fragmental cores were often responsible for the clogging of the drill hole. Oxidized ore veins were found in large numbers and those over 5 cm in width were distributed in the depth ranges of 27.75 to 27.92 m, 32.85 to 33.25 m, 37.90 to 38.05 m, 45.45 to 45.80 m, 64.25 to 64.65 m, 85.50 to 85.70 m, 118.35 to 119.55 m and 120.50 to 128.50 m. The vein parts were heavily oxidized, fragmental and soft. For this reason, core samples were collected from a shorter section so as to achieve better core recovery. However, a slightly lower core recovery was inevitable in fragile porous limonite zones.

[Fall of inner tubes]

When the depth of 35 m was reached, the inner tubes came off the overshot, and fell down to damage the diamond bit. As a result, much difficulty was experienced in raising the drill pipes, but the pipes were safely recovered. The accident happened when a locking sleeve fitted to the overshot touched the mouth of the hole to force the inner tubes out of position.

All the field personnel were warned against a repetition of such an accident.

[Insertion of BW casing pipe]

Caving occurred in open fissures and oxidized ore veins in the depth range of 103.40 to 130.15 m. BW casing pipes were inserted to a depth of 130.15 m to protect the hole wall.

Depth range : 133.15 - 215.25 m

The hole was drilled in this section with BQ-WL diamond bits. The geology of the section consisted primarily of white saccharoidal limestone with numerous weakly oxidized sulfide veins. The veins were attached to the host rock very closely, and the host rock was massive and relatively free from fissures and calcite veins. This permitted a high core recovery to be achieved and facilitated the drilling operation as a whole.

[Standby]

When the drill hole was reached to the depth of 215.25 m including

an extra depth over the planned depth of 212.50 m, the drilling personnel stood by pending the judgement of the geologists. Mineralization effects were observed as far as the depth ranging from 214.30 to 214.80 m. Concluding that the mineralized zone had not been passed, it was decided to drill to a depth of 300 m as in the case of DDH-M1.

Depth range : 215.25 - 256.60 m

The white saccharoidal recrystallized limestone beds continued to the depth of 229.10 m, and a mineralization effect was locally observable. The drilling progressed smoothly.

Beyond the depth of 229.10 m appeared a heavily fractured and in part highly brecciated saccharoidal limestone beds. The brecciated zones and fissures were completely filled with dogtooth calcite.

The drilling progressed without much difficulty, but in some parts the fissures filled with calcite were fractured weakly and there were found some precipitates of brown iron oxide. Core recovery was somewhat lower in those parts.

Depth range : 256.25 - 302.25 m

Beyond the depth of 256.25 m the drill pipes vibrated heavily, which threatened to damage the hole wall in the fracture zones and to induce caving eventually. Pressure on the bit was reduced to control the vibration of the drill pipes, and this resulted in a slower drilling speed. A zone heavily fractured, brecciated and filled with dogtooth calcite continued to the depth of 290.25 m. Weak effects of mineralization were observed in some parts of the fracture zone. Between the depths of 290.25 and 296.25 m lay a rather argillaceous limestone bed intercalated with thinly bedded clay and lacking in fissures. Saccharoidal recrystallized limestone appeared again in the depth range of 296.25 to 302.25 m, but the development of fissures was feeble.

Those beds, though fractured, were filled well with dogtooth calcite veins as earlier described. Although the operating efficiency was more or less reduced, the drilling through this section made good headway on

the whole. Beyond the fracture zone was hardly observed mineralization effect. When the geologists examined the core samples and concluded that the object of the drilling had been accomplished, the operation was terminated after recovering and inspecting the drill pipes and the core samples.

[Fall of inner tubes]

During the descent of the inner tube to the depth of 268.25 m, it fell off the overshot at the depth of 150 m and went through the BQ-WL diamond bit. Attempts were made to raise the BQ-WL drill pipes and to recover the tools. The BQ-WL diamond bit was slightly deformed and caught in the casing pipe end. The drill pipes were raised with much difficulty. The overshot and the inner tube were checked after recovering, but any defect of tools was not found. The cause of the accident was uncertain, but it was conceivable that the inner tube might have hit a slight corrugation in the drill pipe joint and forced the locking sleeve to go off, causing the tube to drop. After the accident, drill pipes were used selectively and the descending speed of the inner tube was reduced. These steps helped to avoid the repetition of this type of accident.

2.6.3 DDH-M3 (Depth : 212.25 m, Vertical)

Depth range : 0.00 - 5.80 m

The section between the surface and the depth of 5.50 m consists of overburden including limestone pebbles, and the next section continuing to the depth of 5.80 m is composed of weathered limestones full of joints. These sections were drilled with a 115 mm metal crown without using water, and after inserting 115 mm casing pipes into the hole, the drilling was performed with NQ-WL diamond bits.

Depth range : 5.80 - 155.80 m

This section consisted of recrystallized limestone beds intercalated locally with thinly bedded argillaceous marl and marly limestone. Fissures filled with dogtooth calcite, fracture zones and brecciated zones were observed. There were also found numerous open fissures

Fig. III-3 Progress Record of Diamond Drilling

DDH-M3 Vertical

Depth M	Drill log	Geology	Drilling hour / meter		Drilling Method		Performance																									Remarks									
			(minute)					Depth of bit change	Hole diameter	Casing diameter	September																														
			10	20	30	40	50				10	11	12	13	14	15	16	17	18	19	20	21	22	23	24	25															
5.80		Gravel, clay and humus					115mm Metal crown	115mm	HWCP	5.80	5.80	Opening hole & collaring on 12th Sep Bit pressure: 1,000~400 kg/cm ² , 250rpm Feed water: 40~50 l/min 1830 Return water: 0 l/min (clean water was used)																									Drilling preparation Transportation of drilling equipment Reaming Bit pressure 500~1,000 kg/cm ² , 250rpm Feed water 40 l/min. Return water 0 l/min (clean water was used)				
20.04							NQ-WL	NWCP			29.30	30.00	Reaming Bit pressure 500~1,000 kg/cm ² , 250rpm Feed water 40 l/min. Return water 0 l/min (clean water was used)																												
50.00								NW				41.25		NQ-WL																											
100.00								NQ				59.25	60.00																												
109.95								131.60				75.45																													
128.10								137.25				91.10	85.00																												
137.25								153.30				109.95	110.00																												
153.30								155.80				128.10	125.00																												
155.80								170.55				137.25	140.00	Below the depth of 155.80 m: Bit pressure: 500~1,000 kg/cm, 250~450 rpm Feed water: 40 l/min Return water: 0 l/min. (clean water was used)																									Drill rod was held due to jamming: HW casing pipe was inserted to pull up the rod and the casing pipe was set as measurement Completion of drilling & dismantling of machines & derrick		
170.55							182.25				155.30	155.80																													
182.25								192.45				170.55																													
192.45								212.25				182.25																													
212.25								212.25				192.45																													
212.25												212.25																													
212.25													212.25																												
212.25																																									
212.25																																									
212.25																																									

accompanied with iron oxide precipitates. These fissures were abundant in the depth ranges of 16.00 to 38.20 m and 140.25 to 146.80 m. At the depth of 16 m a complete lost circulation occurred, and the drilling continued without using water. When the hole was drilled to the depth of 131.60 m, burning of a bit occurred.

[Burning of bit]

The burning probably was caused by a rapid lost circulation due to druse-rich calcite veins stained with iron oxide in the depth range of 131.60 to 132.30 m. Lost circulation was heavy throughout DDH-M3, and the water pressure gauge remained pointing the zero. This is considered one of the reasons to delay discovery of burning of the bit. After the accident, the water supply was increased during the drilling operation.

Heavily fractured and brecciated zones were found between 131.60 m and 137.25 m, and they were well filled with calcite. Relatively stable recrystallized limestone continued from the depth of 137.25 m to the depth of 152.80 m and the drilling progressed smoothly.

[Stuck of drill pipes]

At the depth of 155.80 m the drill pipes were raised about 2 m to lift the inner tube, and attempt was made then to lower the drill pipes to the bottom of the hole. However, the drill pipes were stuck and could not be moved up and down. It was proposed to use a drop hammer and a 10-ton pulling jack were used to move the drill pipes, but a drill pipe adjacent to the mouth of the hole was damaged. Therefore, the idea of using the drop hammer and pulling jack was given up and the hole was reamed with NW casing pipes. At the depth of 153.30 m, all the tools could be recovered with success. Six shifts were required for this operation.

The rod got stuck presumably because sludge could not be washed out properly as the hole was drilled through recrystallized limestone beds containing a limited number of open fissures. After this accident, ample time was spent on cleaning the bottom of the hole before moving the inner tube in order to wash out sludge, when

stable limestone beds were encountered. This precaution helped to prevent the repetition of that sort of accident.

Depth range : 155.80 - 212.25 m

This section consisted of recrystallized limestone accompanied locally with marl. Heavily brecciated fracture zones were encountered in the depth ranges of 157.10 to 163.10 m and 176.25 to 195.0 m, and they were completely filled with dogtooth calcite. The drilling progressed smoothly on the whole, but core recovery was somewhat lower in the limonite-stained marl beds found below the depth of 189.65 m. When the depth of 212.25 m was reached, the geologists concluded that the object of the drill hole had been attained, and the operation was terminated after examining the core samples.

2.6.4 DDH-M4 (Depth : 203.25 m, Vertical)

Depth range : 0.00 - 5.90 m

Since the overburden intermingled with limestone pebbles continued from the surface to the depth of 5.90 m, the hole was drilled with a metal crown without circulating water. NW casing pipes were then inserted and the drilling was continued using NQ*WL diamond bits.

Depth range : 5.90 - 213.25 m

Section below the depth of 5.90 m comprised stable marly limestone and limestone characterized by a very limited number of joints, and drilling water was recovered nearly 100% until the depth of 193.75 m was attained.

Fracture zones bleached and stained with iron oxide were encountered in the depth ranges of 41.25 to 41.95 m, 46.50 to 47.25 m and 130.00 to 198.30 m. However, the fractured zones except the depth range of 130.00 to 198.30 m were filled with calcite veins, and the drilling progressed without experiencing lost circulation. In the depth range of 130.00 to 198.30 m, the fracture zones were filled with calcite veins, but all the drilling water was lost. Therefore, the drilling operation had to be continued under lost circulation. In addition to the calcite veins mentioned above, white calcite veins were found below the depth of 151 m, and were abundant especially below the depth of 198.30 m. They were not

Fig. III-4 Progress Record of Diamond Drilling DDH-M4 Vertical

Depth M	Drill log	Geology	Drilling hour / meter					Drilling Method		Performance					Remarks						
			(minute)					Depth of bit change	Hole diameter	Casing	September					October					
			10	20	30	40	50				26	27	28	29		30	1	2	3	4	5
5.90		Gravel, clay and humus						115mm Metal crown 590	115mm 590	HW C P	Opening hole & collaring on 28th Sep Bit pressure 1,000 kg/cm ² , 250rpm Feed water 40 l/min Return water 0 l/min (clean water was used) Below the depth of 17.25m, 40 l/min of return water was measured										
		Marly limestone, gray-to-dark gray, massive, rarely intercalating black carbonaceous lamina, as well as marl lamina									17.25 Below the depth of 17.25m, 40 l/min of return water was measured										
		Marly limestone, dark gray, thin-to-medium-bedded, intercalating black carbonaceous beds									47.25										
50		Limestone, grayish white, fine-grained, compact, medium-to-thick-bedded, intercalating black thin carbonaceous beds, as well as marl thin beds								NQ -WL	65.25										
											86.25										
		Marly limestone, dark gray, thin-to-medium-bedded, alternating black thin carbonaceous beds									106.55										
100		Marly limestone									106.25										
		Limestone									128.25										
150											149.25										
		Marly limestone, black-to-dark gray, thin-to-medium-bedded, intercalating black thin carbonaceous beds									170.25										
200										185.25 Below the depth of 193.75m, return water was stopped											
203.25							NQ 203.25	203.25		203.25 Dismantling of machines & derrick Completion of drilling & measurement of drilled depth											

at all accompanied by mineralization. When the depth of 203.25 m was reached, the geologists checked the core samples and concluded that the object of the drill hole had been attained. The operation was terminated after inspection of the drill pipes and the core samples.

2.6.5 DDH-M5 (Depth : 220.95 m, Direction : N55°W, -55°)

Depth range : 0.00 - 1.90 m

Since the overburden consisting mainly of limestone gravel continued from the surface to the depth of 1.90 m, the hole was drilled with a 115 mm metal crown without using water. A 115 mm casing pipe was then inserted into the hole and the drilling was continued with NQ-WL diamond bits.

Depth range : 1.90 - 220.95 m

This section consisted of saccharoidal recrystallized limestone interbedded partly with marly parts. It is generally fractured and characterized by a wide distribution of fissures. Heavily brecciated zones were partly formed in the section. Numerous veins were formed in the depth range of 80 to 164.00 m. The fissures and brecciated zones were filled with dogtooth calcite, and the veins were well fitted with the host rocks, no serious problems were encountered in drilling. However, open fissures were found and a total lost circulation occurred at the depth of 2.50 m. Subsequently, the drilling had to proceed under lost circulation. Water was injected into the opening between the drill hole wall and the drill pipe to control its vibration. As the drill hole was inclined, the water failed to circulate properly throughout and the drill pipe vibration tended to increase with an increase of the depth of the hole. Therefore, the rotation speed of the drill pipe had to be reduced as the drilling proceeded. This inevitably resulted in some decline in the drilling efficiency. Since open fissures slightly increased in number below the depth of 90 m, clogging of core samples occurred and a lower core recovery resulted. However, the drilling made a satisfactory progress on the whole. When the hole was drilled to the depth of 220.95 m, the geologists examined the core samples and concluded that the object of the drill hole had been achieved. The operation was terminated after inspecting the drill pipes and the core samples.

3. CONSIDERATION

Diamond drillings of the five drill holes during the current survey were performed with the objectives stated in Section 1.1., Chapter 1. They attained their objectives as described below.

- 1) Each drill hole consisted primarily of limestone beds interbedded partly with marl. In all the drill holes except DDH-M4, rocks were heavily recrystallized, and in some cases it was difficult to presume their origin.

However, the drill hole geology corresponded well on the whole to the surface geology, and thus the drilling work contributed in a large measure toward shedding light on the stratigraphy and structure.

- 2) Structurally, in DDH-M1, DDH-M2, and DDH-M3, the occurrence of conspicuous fracture zones around Kau III unit was confirmed. It also was made clear that the concealed intrusive rock body, whose occurrence had been predicted, would occur at an unexpectedly great depth.
- 3) It was confirmed that the thermal metamorphic zones consist mainly of recrystallized limestone and that large porphyroblastic garnet, wollastonite and hedenbergite occur in some parts of the skarn mineral-bearing recrystallized zones. This will contribute largely toward estimation of the conditions of metamorphism.
- 4) In DDH-M1, DDH-M2, DDH-M3 and DDH-M5, ore bodies of relatively high grade were encountered, which contributed largely to the exploration of the mineralized zone in this area. In DDH-M2 and DDH-M5, primary sulfide ores were locally distributed, and this is an important contribution toward the elucidation of the nature of mineralization.
- 5) In DDH-M4 which was drilled for the purpose of investigating the IP anomalies, carbonaceous limestone and marl were found, and concluded to be the cause of IP anomalies.

Aside from the geological achievements described above, the following measures were taken to solve problems associated with drilling techniques and operational efficiency, thereby facilitating the completion of the entire drilling operations according to schedule.

- 1) In addition to the great distance from the nearest community, many problems such as difficulty in obtaining water, difficulty in procuring equipment and materials, bad road conditions and poor accommodations had been pointed.

However, preparations progressed smoothly and the road conditions were improved to minimize the time required for transportation of personnel and equipment. The base camp was located close to the drilling sites and this helped improve the operational efficiency to a large extent.

- 2) In all the drill holes except DDH-M4, lost circulation occurred even at relatively shallow parts. As a result the drilling operations were continued using fresh water under lost circulation. The wire-line method as applied to such drill holes involve technical difficulties. During the initial stage of the drilling works, there arose troubles such as the drop of inner tubes, burning of bit and stuck of drill pipes due to incomplete washout of sludge. Moreover, vibration of drill pipes resulted in a lower operating efficiency.

However, thoroughgoing investigation on the causes of the troubles was undertaken and appropriate remedial measures taken without delay. In consequence the occurrence of similar accidents was greatly reduced during the rest of the drilling work period.

PART IV

CONCLUSION

1. CONCLUSION

As described in preceding chapters, the hydrothermal silver-bearing copper ore deposits of vein-type related closely to the intrusive rock of Neogene are distributed in the limestone-predominant calcareous sedimentary rocks of the Aurora formation in this area. These ore deposits are controlled by the concealed intrusive igneous rock, the thermal metamorphic zone, the younger and older fractures, etc. It is also assumed that the lower extension of these ore deposits might be expected to have some bonanzas at the horizons of the La Peña and the La Cupido formations.

In addition, the formation of ore deposits of Mina la Morena and Mina el Refugio localized on the piedmont of the northeastern part of the Sierra la Morena is also considered to have taken place in relation to the same mineralization.

From these aspects on the mineralization and geology, it will be recommended to continue the exploration further.

It will be also recommended to reexamine the El Valcan area and the alteration zone in the Sierra de Cruces area (around Mina Libertad and the Noria del Picacho dome) which have similar geological environments with this area, if the exploration in this area results in success.

2. FUTURE EXPLORATION

The future exploration should be directed to make the confirmation of lower extension of main mineralized zones found in the Aurora formation.

(1) Exploration in the horizon of the Aurora formation

Following veins and mineralized zones are to be explored:

- i) Lower part of the skarn minerals-bearing recrystallized zone
- ii) Mineralized zone in the eastern part of the thermal metamorphic zone
- iii) Veins and mineralized zones of NE 2, 3 and 4 in the northeastern part of the thermal metamorphic zone

- iv) Mineralized zone of N4 in the northern part of the thermal metamorphic zone

For the exploration, special attentions described below are to be taken.

- i) These recommended zones are distributed in the high copper zone where the most prominent mineralization are observed in the area.
- ii) Comparatively large-scale ore bodies occur mainly in the outer margin and the periphery of the thermal metamorphic zone.
- iii) The sericite-quartz rock seems to be related closely to ore bodies and is highly mineralized in general.

In addition, the "P" anomaly of IP survey is also recommendable, because it is located on the geophysical discontinuity inferred to be extension of a fault in which NE-SW vein occurs.

- (2) Exploration for the horizons of the La Peña and the Cupido formations

The two formations are deeply seated beneath the area, which results in great difficulty for the drilling exploration. It is considered, however, to be very important for the evaluation of economic potential of the ore deposits in the area because of possible occurrence of bonanzas in these formations.

The area in which the Kau I unit of the Aurora formation is distributed as window has the advantage of shorter drill length to these horizons, where the top of the Cupido formation is estimated to be reachable at the depth of about 300 m from the surface. In the southwestern part of the area, however, it is estimated to be much deeper, and a depth of about 600 to 800 m would be necessary.

In this exploration for deeper horizons, some problems important and essential for evaluating the economic potential of the ore deposits in this area, such as the concealed intrusive igneous rock and the relation between skarnization and mineralization, should be studied together with the mineral exploration.

For future exploration as mentioned above, it is necessary to consider that various structures concerning the mineralization in this area, such as concealed intrusive rock body, thermal metamorphic zone, mineralized zone, etc., tend to plunge to the northwest or north-northwest, and that the ore deposits in this area are probably formed under the same activity of mineralization as those located to the north of the area such as Mina la Morena and Mina el Refugio. Also the electric potential method using drill holes would be useful to obtain the structural information of the ore bodies.

REFERENCE

- Armstrong, R.L. & McDowell, W. G. (1974): Proposed refinement of the Phanerozoic time scale, Abstract, Int. Mig. Geochron. Cosmochron. Isotope Geol., Paris.
- J.I.C.A. & M.M.A.J. (1976): Report on geological survey of the Coahuila area, northern Mexico, phase I.
- _____ (1977): Report on geological survey of the Coahuila area, northern Mexico, phase II.
- _____ (1978): Report on aeromagnetic survey of the Coahuila area, northern Mexico, phase III.
- Miyashiro, A. (1965): Metamorphic rock and metamorphism (in Japanese), Iwanami Press.
- Smirnov, V.C. (1969): Geological study of mineral deposits.
- Sunagawa, I. (1953): Variation of crystal habit of calcite, with special reference to the relation between crystal habit and crystallization stage, Rep. no.155, Geological Survey of Japan.

(2) 参考 (供試器具)

A

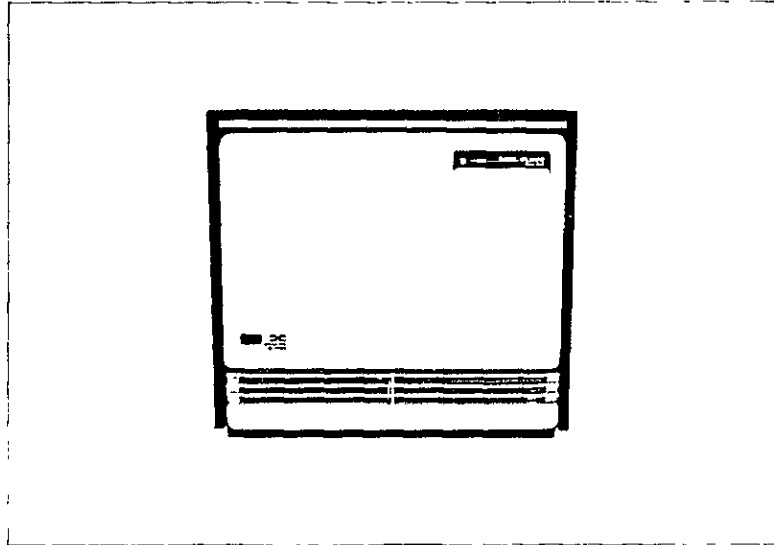


Photo. 1

B

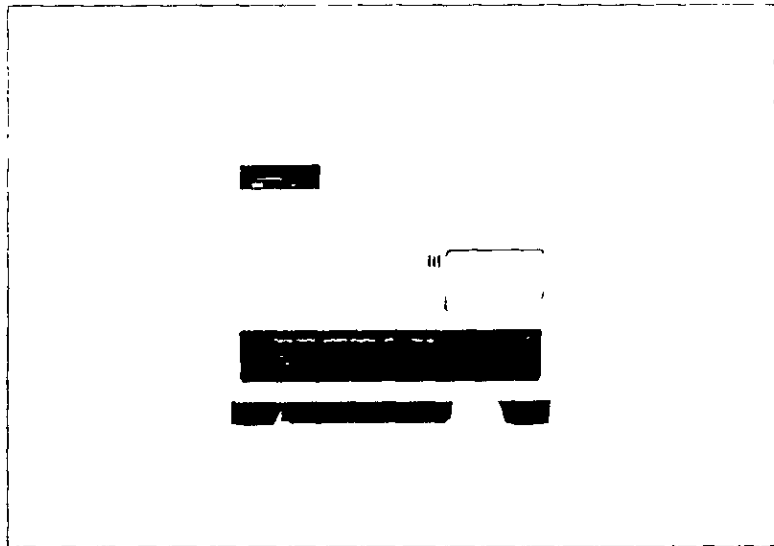


Photo 2

C

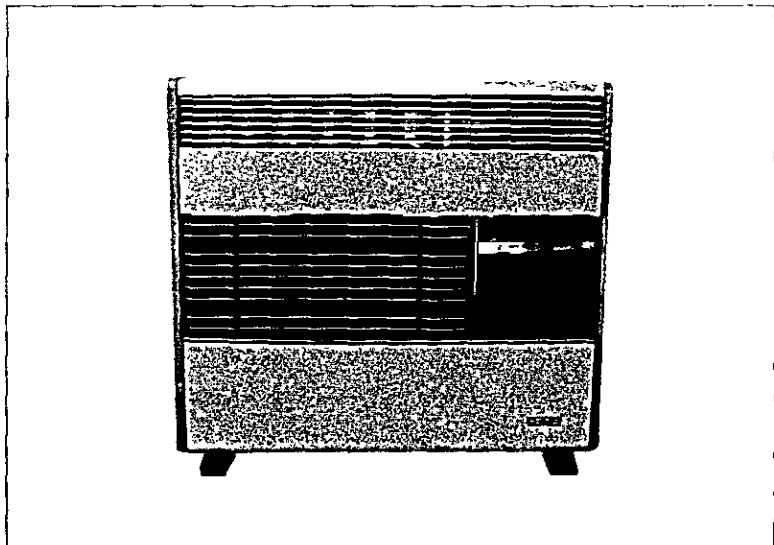


Photo 3

APPENDICES

PART I
GEOLOGICAL SURVEY

APX. I-1	Geological sketches	A-1
APX. I-2	Chemical analyses of surface ore samples	A-9
APX. I-3-(1)	Microscopic observations of thin sections of surface samples	A-19
APX. I-3-(2)	Photomicrographs of thin sections of surface samples	A-27
APX. I-4-(1)	Microscopic observations of polished sections & electron probe microanalyses of surface samples	A-32
APX. I-4-(2)	Photomicrographs, secondary electron images and characteristic X-ray images of polished sections of surface samples	A-39
APX. I-4-(3)	Qualitative analysis of ore minerals of surface samples by electron probe microanalyzer	A-54
APX. I-5-(1)	Detected minerals by X-ray diffractions	A-55
APX. I-5-(2)	Charts of X-ray diffractions	A-56
APX. I-6	Chemical analyses and X-ray diffraction data of natrojarosite	A-58
APX. I-7	K-Ar datings and whole rock chemical analyses	A-59

APX. I-1 GEOLOGICAL SKETCHES

SKA - 1, 2, 3, 4, 5

SKC - 1, 2, 3

SKE - 1, 2

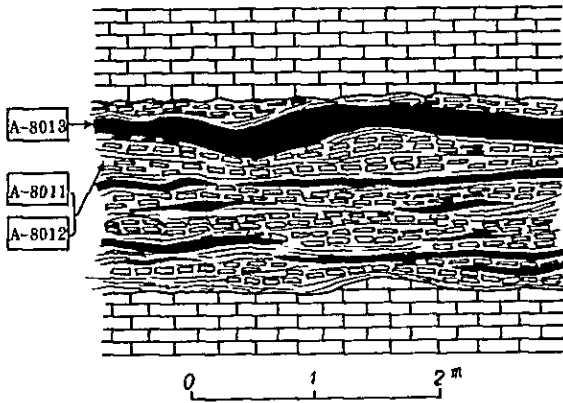
SKG - 1, 2, 3




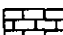
* Coordinates: refer to PL. I-1

SKA - 1

* Coordinates

N: 3123402
E: 647124

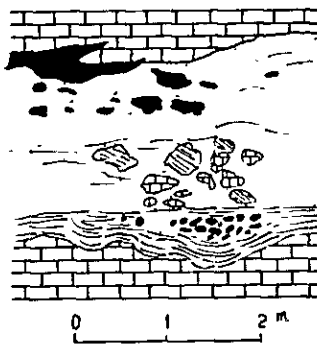




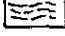
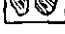
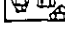
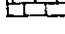
-  banded hematite and limonite
-  hematite and limonite networks/stringers
-  banded granular calcite
-  thickly bedded limestone

SKA - 2

* Coordinates

N: 3123898
E: 646208



-  black hematite
-  fine-grained hematite and calcite
-  banded hematite
-  aggregated crystalline calcite
-  limestone relict
-  limestone

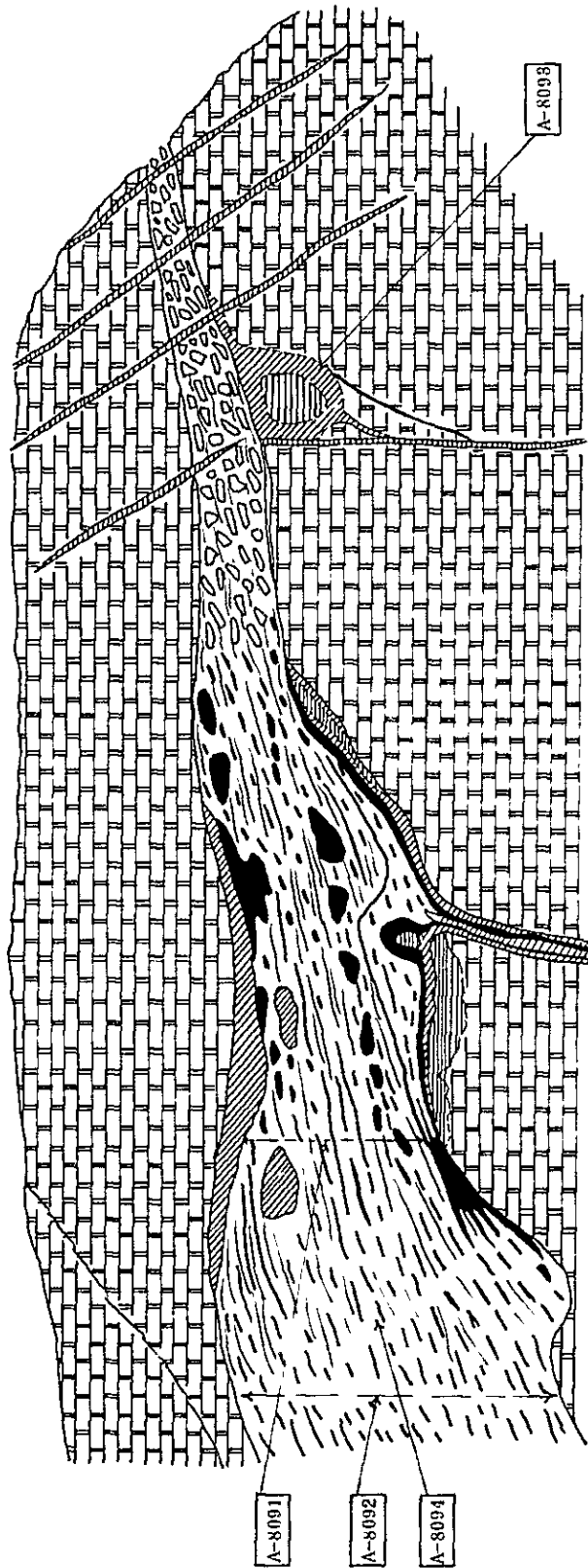
SKA - 3

* Coordinates



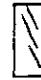


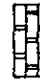

N: 3124004

E: 647933

*



0 0.5 1 m

-  green copper-minerals
-  hematite
-  hematite stringer networks
-  green copper minerals and azurite
-  granular calcite
-  transparent saccharoidal limestone
-  minor fault

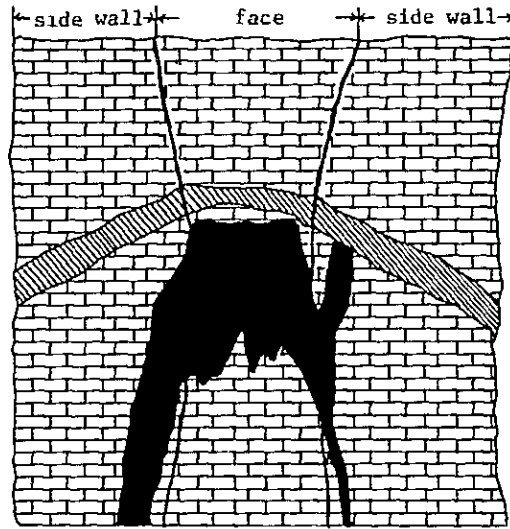
SKA - 4



* Coordinates


(Mina La Diana shaft)

N:3124671

E: 648262



 manto vein type hematite with rare green copper-minerals
 limestone

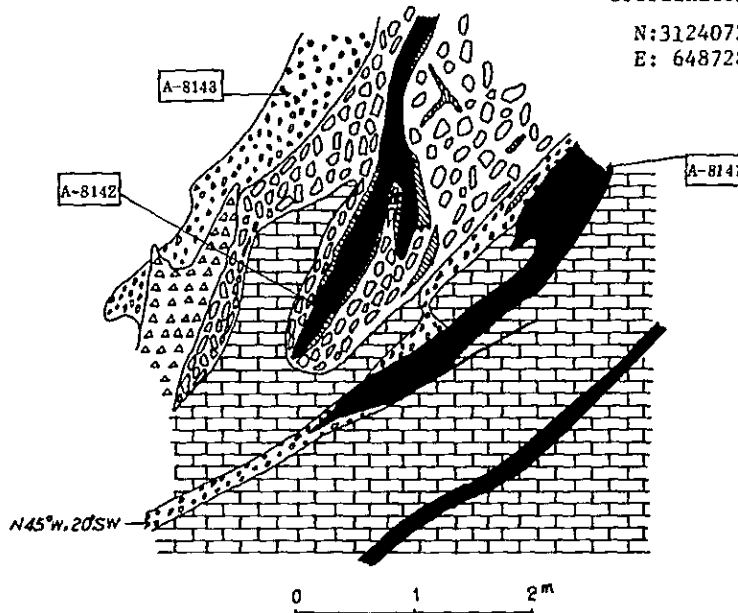
 manto type green copper-minerals and hematite (N55°W, 28SW)


SKA - 5

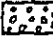
* Coordinates


N:3124072


E: 648728

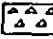



 banded limonite

 druse filled with calcite and iron oxide

 green copper-minerals

 coarse-grained calcite

 druse

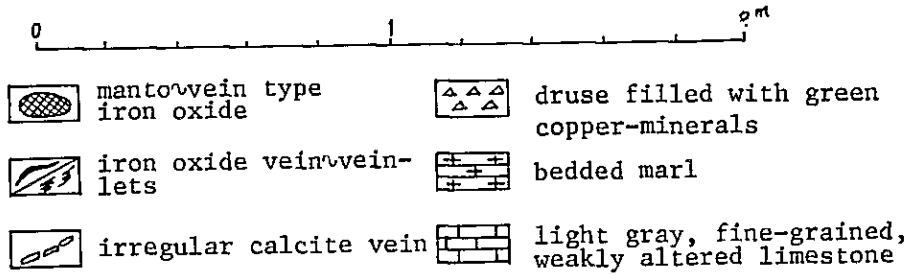
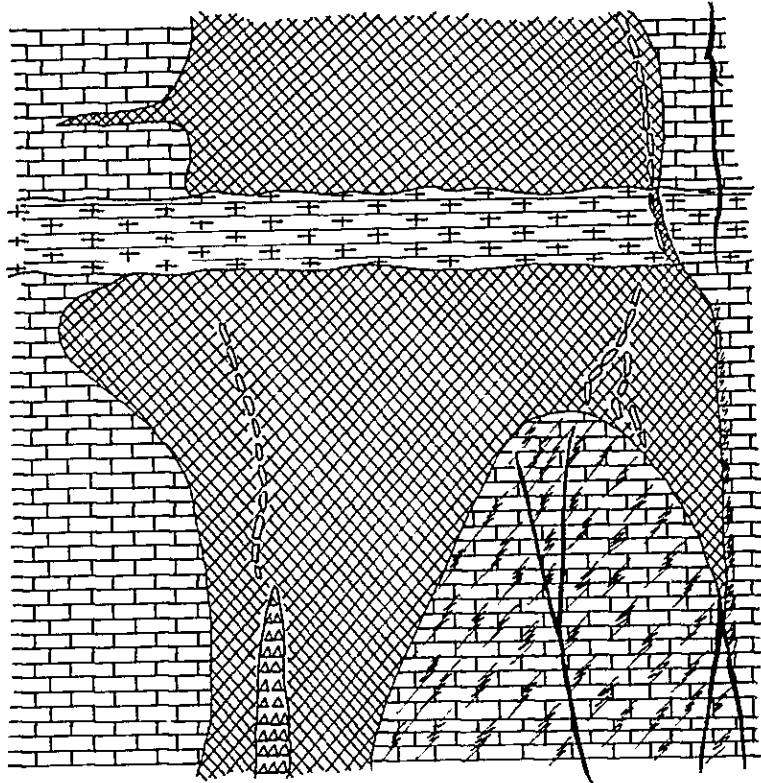
 limestone (bedding: N45°W, 20°SW)

SKC - 1

* Coordinates

N: 3124204

E: 648327

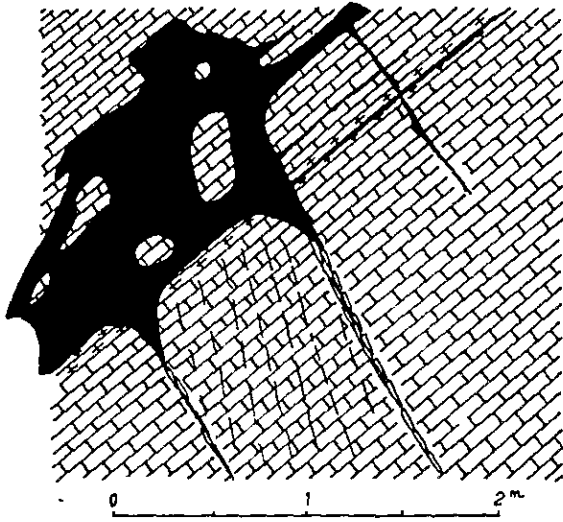





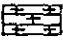
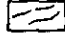
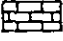
SKC - 2

* Coordinates

N:3124797

E: 648389



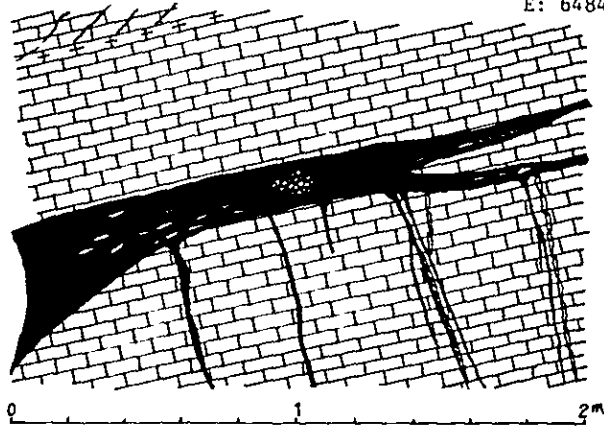
- | | |
|---|--|
|  hematite and calcite vein with low-grade iron oxide ore |  calcite vein stained by limonite |
|  hematite and limonite |  marl or marly limestone |
|  fractures filled with iron oxide |  limestone |


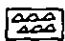

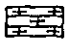

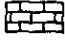

SKC - 3

* Coordinates

N:3124828

E: 648410

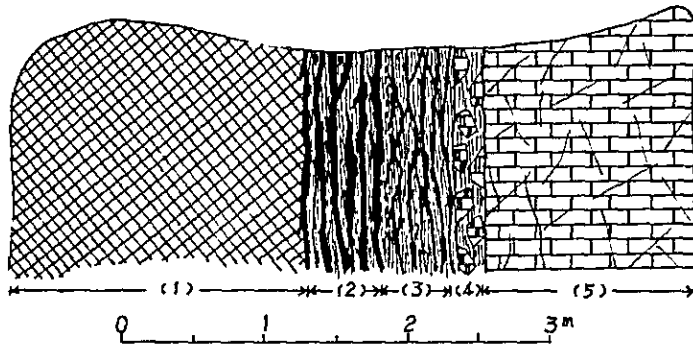






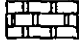
- | | |
|---|--|
|  manto type iron oxide |  druse (hard silicified part) |
|  iron oxide vein |  oxidized marl |
|  calcite vein |  limestone |
|  green copper-minerals | |

SKE - 1 * Coordinates

N: 3124223

E: 646948



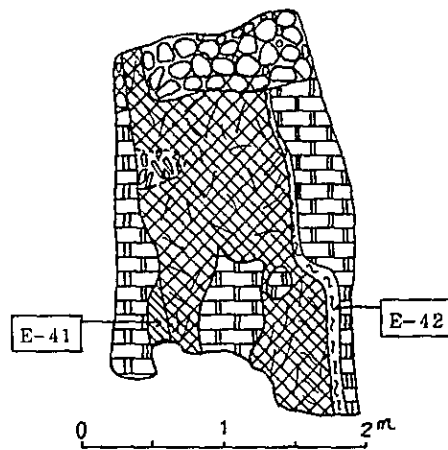
- (1)  almost pure hematite (very fine-grained)
- (2)  hematite and calcite
- (3)  calcite veinlets > hematite
- (4)  calcite veinlets in brecciated limestone
- (5)  limestone with calcite veinlets along cracks



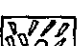


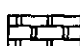
SKE - 2

* Coordinates

N: 3124349

E: 648354



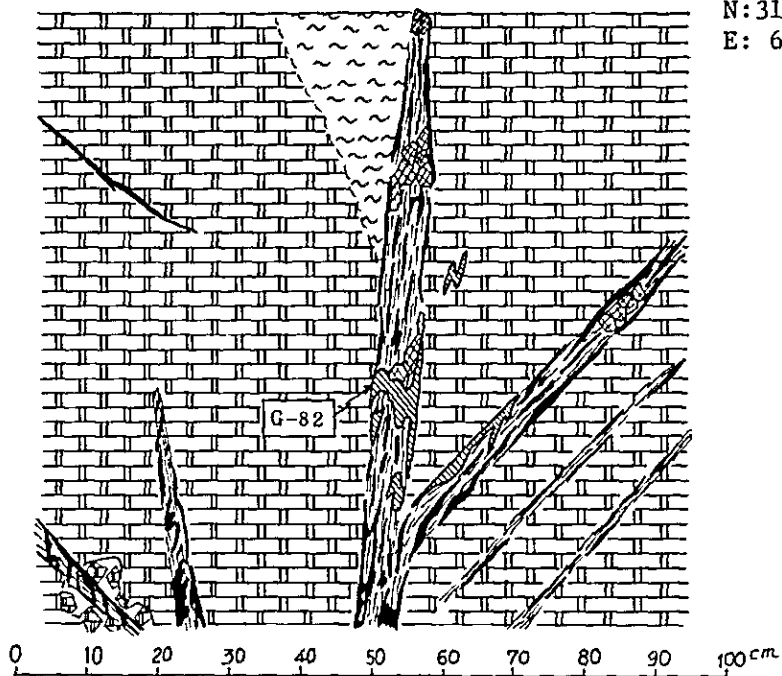
-  green copper-minerals and hematite
-  hematite with calcite networks
-  calcite networks with brecciated hematite
-  whitish clayey pulverulent limestone
-  overburden
-  recrystallized limestone



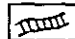


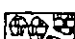
SKG - 1

* Coordinates

N: 3123938

E: 647780

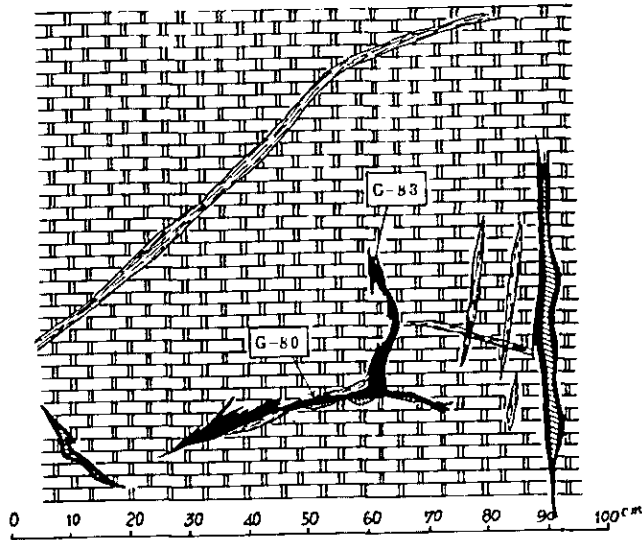





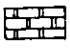
- | | |
|---|--|
|  iron oxide vein |  crystalline calcite vein |
|  garnet skarn vein |  sheared, fractured part |
|  brecciated recrystallized limestone |  recrystallized limestone |

SKG - 2

* Coordinates

N: 3123930
E: 647808

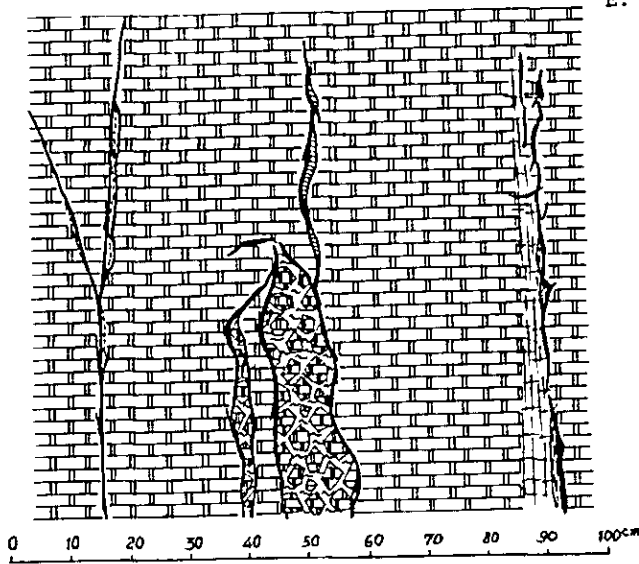









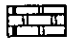
- | | | | |
|---|-----------------------|---|---|
|  | iron oxide vein |  | crystalline calcite vein |
|  | green copper-minerals |  | recrystallized limestone
(bedding N20°E, 20°W) |

SKG - 3

* Coordinates

N: 3123920
E: 647768



- | | | | |
|---|--|---|--|
|  | iron oxide vein |  | calcite vein |
|  | green copper-minerals |  | quartz vein |
|  | fractured and filled
with iron oxide nets |  | brecciated recrystallized
limestone |
|  | brecciated clayey part |  | recrystallized limestone |

APX. I-2

CHEMICAL ANALYSES OF SURFACE ORE SAMPLES

APX. I-2 CHEMICAL ANALYSES OF SURFACE ORE SAMPLES

No.	Sample No.	Coordinates		Occurrence			Chemical analyses						Remarks	
		E	N	Minerals and type	Direction	Width (m)	Scale of mineralization	Au g/t	Ag g/t	Cu %	Pb %	Zn %		
1	A-7271 A	647645	3124147	Iron oxide manto	N30°40'E, 30°SE	0.2	0.2m x 60m	tr.	8.7	0.05	0.01	0.01	0.01	
2	A-7272 A	647677	3124120	Green copper mineral - calcite veinlets		2	2 x 2	tr.	59.3	3.56	0.01	0.01	3.27	
3	A-7273 A	647743	3124100	Green copper mineral ore (floats)			20 x 20	4.4	26.1	1.58	0.03	0.03	1.15	
4	A-7274 APE	647873	3123990	Hematite-green copper mineral ore (stock pile)			2 x 2 x 2	0.5	255.6	8.16	0.02	0.02	0.21	
5	A-7311 A	647685	3122910	Calcite-green copper mineral vein	N50°E, 60°NW	2.5	2.5 x 18	tr.	1.6					
6	A-8011 APE	647125	3123402	Hematite-calcite manto	N60°W, 20°SW				5	0.21	0.01	0.01	0.04	cf. geological sketch SKA-1
7	A-8012 A	ditto	ditto	ditto	ditto	3	3 x 30	tr.	tr.	0.01	0.01	0.01	0.01	ditto
8	A-8013 A	ditto	ditto	ditto	ditto			tr.	1.3					ditto
9	A-8031 A	646938	3123526	Iron oxide vein	N45°E	5	5 x 20	tr.	206.5	0.03	0.03	0.03	0.04	
10	A-8071 A	646210	3123898	ditto	N82°W	1.2	2 x 40	0.7	1.9	0.02	0.01	0.01	0.02	cf. geological sketch SKA-2
11	A-8081 A	647993	3123973	Iron oxide-fluorite- calcite veinlets	E-W	2	20 x 20	tr.	21.7	0.01	0.03	0.03	0.03	
									3	0.95	0.01	0.01	0.03	

In case that two analytical results are described in the column of chemical analyses, the upper and the lower are analyzed in Japan and in Mexico respectively.

No.	Sample No.	Coordinates		Occurrence			Chemical analyses					Remarks	
		E	N	Minerals and type	Direction	Width (m)	Scale of mineralization	Au g/t	Ag g/t	Cu %	Pb %		Zn %
12	A-8091 A	647935	3124005	Iron oxide-green copper mineral manto	N50°W, 10°SW			0.8	133.9	2.01	0.01	0.04	cf. geological sketch SKA-3
13	A-8092 A	ditto	ditto	Iron oxide-calcite manto	ditto			2.6	62.7	0.24	0.01	0.18	ditto
14	A-8093 A	ditto	ditto	Green copper mineral manto	ditto	1	1 x 4	5.8	131.2	4.53	tr.	0.07	ditto
15	A-8094 A	ditto	ditto	Iron oxide-calcite manto	ditto			1.2	108.7	0.06	0.01	0.003	ditto
16	A-8095 APE	ditto	ditto	Iron oxide-calcite-green copper mineral manto	ditto			1.6	757.6	5.57	0.09	1.05	ditto (Sampled from an ore stock pile)
17	A-8096 A	648263	3124086	Iron oxide-calcite-green copper mineral vein	N50°E	2		0.7	38.4	5.25	0.05	1.57	
18	A-8098 A	648250	3124074	Iron oxide-calcite-green copper mineral ore (stock pile)			40 x 40	1.1	545.4	7.90	0.03	19.50	
19	A-8099 A	ditto	ditto	ditto				0.6	413.9	1.68	0.03	4.30	
20	A-80910 APE	648272	3124074	Calcite-iron oxide-green copper mineral vein	N60°E	2		tr.	27.9	8.03	0.02	0.25	Sampled from an ore stock pile
21	A-8101 A	648340	3124095	Iron oxide-green copper mineral vein	N30°-50°E, 60°NW			tr.	27.9	5.83	0.04	0.72	ditto
22	A-8102 AP	ditto	ditto	ditto	ditto	2	2 x 30	8	8	2.42	0.02	0.16	
										0.18	0.05	0.31	

No.	Sample No.	Coordinates		Occurrence			Chemical analyses						Remarks
		E	N	Minerals and type	Direction	Width (m)	Scale of mineralization	Au g/t	Ag g/t	Cu %	Pb %	Zn %	
23	A-8103 APE	648340	3124095	Iron oxide-green copper mineral vein				2.0	545.4	2.40	0.16	2.08	
24	A-8104 AP	648248	3124150	ditto	N80°W	0.3	0.3 x 15	tr.	34.8	4.79	0.02	3.06	
25	A-8105 APE	648273	3124670	ditto	N50°E	0.1 ^v 0.2	20 x 30	3.1	9,090.9	16.06	0.16	0.19	cf. geological sketch SKA-4
26	A-8141 A	648272	3124074	Banded iron oxide manto	N45°W, 20°SW	0.6		1.9	13.4	0.17	0.004	0.08	cf. geological sketch SKA-5
27	A-8142 A	ditto	ditto	ditto	ditto	0.3	4 x 5	tr.	69.6	0.38	0.01	0.04	ditto
28	A-8143 A	ditto	ditto	Iron oxide and calcite filling a druse	ditto	0.5		0.5	43.5	0.15	0.02	0.04	ditto
29	A-8147 A	648250	3124074	Iron oxide-green copper mineral vein	ditto	0.3		tr.	59.3	7.71	0.003	21.75	
30	C-2 A	647695	3124228	Iron oxide-green copper mineral veinlets	E-W	0.1	0.1 x 30	tr.	46.0	3.86	0.10	6.11	
31	C-3 A	647752	3124183	Calcite-green copper mineral vein				tr.	26.6	0.66	0.03	0.02	
32	C-4 A	648558	3123763	Iron oxide veinlets		0.3	0.3 x 8	2.7	21.8	0.02	0.02	0.03	
33	C-5 A	648270	3123965	Iron oxide (after pyrite) - calcite vein	N60°E, 90°	4	4 x 30	0.9	4.8	0.02	0.02	0.01	

No.	Sample No.	Coordinates		Minerals and type	Occurrence		Chemical analyses						Remarks
		E	N		Direction	Width (m)	Scale of mineralization	Au g/t	Ag g/t	Cu %	Pb %	Zn %	
34	C-7 A	647230	3123656	Iron oxide (after pyrite)-green copper mineral vein	N70°E, 90°	0.15	0.15 x 80	tr.	4.8	0.64	0.03	0.04	
35	C-8 A	647045	3123573	Iron oxide (after pyrite)-calcite vein	N55°E	6	6 x 60	tr.	2.4	0.15	0.02	0.04	
36	C-9 A	646923	3125008	Iron oxide manto		0.2~0.9	10 x 15	0.8	11.5	0.05	0.05	0.09	
37	C-10 A	647250	3125250	Iron oxide (after pyrite)-calcite vein	N55°E, 80°E	1	20 x 0.8	tr.	4.8	0.08	0.02	0.08	
38	C-11 A	647490	3125197	Iron oxide manto	N30°E, 18°SE	1	40 x 40	tr.	7.2				
39	C-13 A	647795	3125170	Iron oxide-calcite-green copper mineral veinlets	N30°E		140 x 140	0.8	657.0	3.11	0.02	2.21	
40	C-15 A	647158	3124522	Iron oxide-calcite manto	N10°E, 10°SE	2	2 x 100	1.8	14.5	0.08	0.03	0.16	
41	C-16 A	647310	3124895	Iron oxide-silicate gossan			4 x 25	tr.	tr.	0.002	0.01	0.05	
42	C-19 A	648383	3124832	Iron oxide-green copper mineral vein	N30°E	0.8~ 2	10 x 60	2.5	131.4	4.79	0.08	0.83	
43	C-20 A	648367	3124785	Iron oxide-green copper mineral vein	N80°E, 45°SE	1.2	1.2 x 10 x 6	1.0	131.4	4.92	0.70	0.39	
44	C-21 AT	648273	3124670	ditto				1.5	481.8	5.44	0.37	0.22	
								56	6.99	0.08	0.08	0.17	

No.	Sample No.	Coordinates		Occurrence			Chemical analyses						Remarks	
		E	N	Minerals and type	Direction	Width (m)	Scale of mineralization	Au g/t	Ag g/t	Cu %	Pb %	Zn %		
45	C-22 A	648430	3124860	Iron oxide-green copper mineral vein	N44°E, 50°-67°SE	0.8	8 x 40	1.5	43.8	1.55	0.03	1.32		
46	E-2 A	647623	3123928	ditto	N55°E	0.6	0.6 x 12	tr.	7.2	1.46	0.03	4.11		
47	E-3 A	647740	3123843	Iron oxide vein	N65°E, 90°	0.5 ^v 2	0.5 x 70		5	0.18	0.01	0.21		
48	E-4 A	647700	3123740	ditto	N60°E	2	2 x 6	tr.	4.8	0.04	0.03	0.04		
49	E-5 A	647502	3123758	ditto	E-N, 90°	0.5 ^v 2	0.5 x 20		6	0.04	0.02	0.04		
50	E-7 AP	647515	3123770	Iron oxide-green copper mineral vein	E-N, 90°	1.5	1.5 x 10	0.5	197.1	2.98	0.02	4.06		
51	E-8 A	647335	3123872	Iron oxide vein	N70°E, 45°NW	0.8	0.8 x 5		3	0.01	0.03	0.05		
52	E-9 A	647238	3123947	ditto	N3°E, 60°NW	0.5	0.5 x 10	tr.	3.6					
53	E-11 A	647044	3124072	ditto	N60°E, 70°NW	1	1 x 40		2	0.002	0.01	0.01		
54	E-13 A	646885	3124155	Iron oxide manto	N80°E, 20°SE	1	1 x 5 x 5		3	0.01	0.03	0.47		
55	E-14 AP	646865	3124183	Iron oxide vein	N10°W	4	4 x 12	0.5	tr.	0.001	0.01	0.01		
								8		0.01	0.10	0.01		

No.	Sample No.	Coordinates		Occurrence			Chemical analyses						Remarks	
		E	N	Minerals and type	Direction	Width (m)	Scale of mineralization	Au g/t	Ag g/t	Cu %	Pb %	Zn %		
56	E-15 A	646840	3124235	Iron oxide vein	N30°E	2	2 x 10			4	0.06	0.01	0.05	
57	E-17 A	646865	3124310	ditto	N-S, 50°W	1	1 x 3	0.4	tr.	3	0.04	0.01	0.04	
58	E-18 A	646945	3124223	ditto	N40°E, 90°	3.5	3.5 x 10			3	0.01	0.002	0.05	cf. geological sketch SKE-1
59	E-20 A	647063	3124278	ditto	N55°E, 90°	0.5	0.5 x 2	tr.		6	0.02	0.03	0.01	
60	E-21 A	647105	3124207	Iron oxide manto	N35°W, 15°SW	0.3	0.3 x 20			2	0.002	0.01	0.01	
61	E-22 A	648030	3125035	Iron oxide vein	N30°W, 90°	2	2 x 10	tr.		5	0.06	0.01	0.23	
62	E-23 A	647818	3125203	Iron oxide vein and manto	N38°W	3	3 x 3			10	0.05	0.02	0.33	
63	E-26 A	648235	3124807	Iron oxide-green copper mineral vein	N30°E, 70°SE	0.2	0.2 x 10	6.6		613.2	5.44	0.14	0.79	
64	E-32 A	647093	3123612	Iron oxide vein	N60°E	2	2 x 40	tr.		16	4.24	0.09	0.73	
65	E-34 A	647115	3123725	ditto	N50°E, 90°	4	4 x 30			4	0.01	0.01	0.03	
66	E-35 A	647192	3123685	Iron oxide manto	N50°E, 20°SE	0.6	0.6 x 15 x 15	tr.		7	0.05	0.03	0.06	
										tr.	0.001	0.01	0.01	
										5	0.02	0.05	0.04	

No.	Sample No.	Coordinates		Occurrence				Chemical analyses					Remarks		
		E	N	Minerals and type	Direction	Width (m)	Scale of mineralization	Au g/t	Ag g/t	Cu %	Pb %	Zn %			
67	E-36 A	646718	3123543	Iron oxide vein	N70°W	5	5 x 8	tr.	1.0	0.01	0.003	0.01			
68	E-37 A	648526	3124173	Iron oxide manto and vein	N45°W, 25°SW	0.8	0.8 x 20	tr.	1.0	0.02	0.01	0.03			
69	E-40 A	648350	3124348	Iron oxide-green copper mineral vein	N8°W, 80°NE	1.1	1.1 x 3	0.8	39.4	4.66	0.001	0.20			cf. geological sketch SKE-2
70	E-41 A	ditto	ditto	ditto (iron oxide part)	ditto	ditto	ditto	4.6	1.4	0.08	0.04	0.07			ditto
71	E-43 A	648306	3124392	ditto	N55°E	0.35	0.35 x 5	tr.	394.2	25.00	0.01	0.51			
72	G-1 A	647625	3124060	Iron oxide (after pyrite)-green copper mineral vein	N35°E	max.2 ave.1	1 x 40	tr.	13.6						
73	G-3 A	647712	3123915	Iron oxide-green copper mineral ore (floats)			2 x 2	1.3	131.4	4.4	0.01	0.22			
74	G-5 A	647740	3123903	Iron oxide (after pyrite) vein	N55°E	0.4	0.4 x 30	tr.	4.5						
75	G-9 A	648150	3123676	Iron oxide manto with druse-filling calcite		1	1 x 1	tr.	tr.	0.01	0.02	0.04			Sampled from a prospect
76	G-13 A	647787	3123880	Iron oxide-green copper mineral vein	N50°E	0.5	0.5 x 70	tr.	3.0						
77	G-14 A	647585	3124000	ditto	N50°E	0.5	0.5 x 5	0.5	100.7	5.18	0.01	0.39			
								10	2.16	0.002	0.02	0.36			

No.	Sample No.	Coordinates		Occurrence			Chemical analyses						Remarks	
		E	N	Minerals and type	Direction	Width (m)	Scale of mineralization	Au g/t	Ag g/t	Cu %	Pb %	Zn %		
78	G-25 A	647663	3123823	Iron oxide-calcite vein	N70°E	2	2 x 3	tr.	1.4	0.02	0.004	0.01		
79	G-28 A	647865	3124703	ditto	N36°E, 90°	2	2 x 70	1.0	12.2	0.02	0.004	0.02		
80	G-29 A	647397	3125015	Iron oxide vein	N34°E	1.5	1.5 x 10	tr.	0.9	0.09	0.003	0.13		
81	G-30 AP	648195	3125065	Iron oxide manto	N10°E, 17°SE	0.7	0.7 x 3	1.8	15.3	0.04	0.004	0.68		
82	G-31 A	648222	3125072	Iron oxide vein	N30°E	0.4	0.4 x 5	1.5	91.8	0.13	0.01	0.02		
83	G-32 A	648245	3125025	ditto	N30°E	3.5~ 4	4 x 10	tr.	4.4	0.03	0.004	0.03		
84	G-34 A	648050	3125175	Iron oxide-green copper mineral-vein	N18°W, 60°SW	2	2 x 10	0.8	0.7					
85	G-38 A	647130	3124068	Iron oxide-green copper mineral-silicate vein	N50°E, 90°	2	2 x 20		10	0.14	0.03	0.47		
86	G-40 A	646822	3124227	Iron oxide ore (floats)			6 x 15	4.1	4.6	0.05	0.01	0.03		
87	G-41 A	646920	3124072	Iron oxide vein	N20°E, 60°SE	2	2 x 35	tr.	0.7	0.02	0.01	0.01		
88	G-44 APX	646950	3123552	Jarosite vein and manto	N60°E, 60°SE	2~3	20 x 100	tr.	27.5	0.02	0.003	0.04		
								8	8	0.05	0.01	0.03		

No.	Sample No.	Coordinates		Occurrence			Chemical analyses						Remarks	
		E	N	Minerals and type	Direction	Width (m)	Scale of mineralization	Au g/t	Ag g/t	Cu %	Pb %	Zn %		
89	G-45 A	646998	3123545	Iron oxide manto	N10°~20°E	5~6	20 x 100	0.4	6.1	0.04	0.03	0.04		
90	G-67 A	648375	3124148	Iron oxide vein	N45°E, 90°	1.5	1.5 x 20	2.9	56.2	0.08	0.02	0.37		
91	G-69 A	648412	3124183	Calcite-iron oxide vein-to-networks	N45°E	0.6	0.6 x 20	0.5	15.3	0.11	0.01	0.54		
92	G-72 A	648062	3125203	Iron oxide-calcite vein	N30°W	4	10 x 60	0.6	189.8	0.13	0.01	0.31		
93	G-80 A	647808	3123928	Green copper mineral vein	N50°~60°E	0.1	1.5 x 1.5	2.4	117.2	2.46	0.01	0.02		cf. geological sketch SKG-2
94	G-82 APT	647782	3123935	Garnet-iron oxide vein-to-veinlets	N82°E, 65°E	0.1	1.5 x 1.5	tr.	28.6					cf. geological sketch SKG-1
95	G-83 A	647808	3123928	Iron oxide-green copper mineral vein	N50°~60°E	0.1	1.5 x 1.5	tr.	2.3	0.91	0.01	0.02		cf. geological sketch SKG-2
96	G-85 AP	647885	3124032	Iron oxide-jarosite-green copper mineral vein	N50°E	2.5~3	2.5 x 70	0.5	12.7	0.26	0.06	0.05		
97	G-86 AT	647815	3123965	Garnet-iron oxide-green copper mineral vein	N50°E	0.3	0.3 x 8	9.7	18.8	0.45	tr.	0.25		
98	G-87 A	647772	3123868	Iron oxide-quartz vein	N55°E	0.9	0.9 x 50	tr.	27.5					
99	S-1 A	648339	3123678	Iron oxide vein-to-veinlets	N25°E	0.1	10 x 15		5	0.08	0.003	0.01		

No.	Sample No.	Coordinates		Occurrence			Chemical analyses					Remarks	
		E	N	Minerals and type	Direction	Width (m)	Scale of mineralization	Au g/t	Ag g/t	Cu %	Pb %		Zn %
100	S-2 A	648189	3123715	Iron oxide vein	N35°E	1	1 x 15		2	0.01	0.05	0.01	
101	S-3 A	648053	3123808	ditto	N65°E	1	1 x 25		4	0.02	0.004	0.01	
102	S-6 A	647360	3124280	ditto	N23°E	0.4	0.4 x 8		4	0.004	0.004	0.01	
103	S-7 A	647533	3124155	Iron oxide-calcite vein	N-S	0.8	0.8 x 20		11	0.13	0.10	0.02	
104	S-10 A	647208	3124702	Iron oxide vein	N58°E	1	1 x 40		3	0.01	0.004	0.01	

APX. I-3-(1)
MICROSCOPIC OBSERVATIONS
OF THIN SECTIONS
OF SURFACE SAMPLES

No.	Sample No.	Coordinates		Occurrence	Rock	Macroscopic observations	Microscopic observations
		E	N				
1	A-7312 T	647470	3123067	Aurora F. (Kau IX)	Marl (fossiliferous).	Black, fine-grained, compact, laminated, partly decolored.	Very fine-grained, anhedral granular calcite (0.01-0.02mm) predominates. Small amounts of acicular-to-flaky quartz (<0.01-0.02mm), anhedral limonite(after pyrite, 0.1mm), and spherical-to-arcuate fossil trace (<0.2mm) are scattered. A zonal sedimentary structure is clearly observed by alternating calcite-rich band and quartz-rich band. Fossil traces are replaced by calcite. Recrystallization may not be recognized.
2	A-8032 T	646938	3123526	Aurora F. (Kau XIV)	Limestone (fossiliferous).	Dark gray, fine-grained, compact, massive, stylolite-structured.	Fine-grained, anhedral granular calcite (0.01-1mm) predominates. Small amounts of long prismatic, spindle-shaped, hexagonal, flaky, or anhedral quartz (<0.3mm), fossil trace (<0.3mm), and rare limonite(after pyrite, <0.02mm) are scattered. Fossil traces are filled with calcite. In a stylolite band, quartz predominates. Calcite microveinlets (<0.05mm) penetrate the host rock. Recrystallization may not be recognized.
3	A-8033 T	646697	3123696	Aurora F. (Kau XIII)	Marl (fossiliferous).	Black, fine-grained, compact, massive.	Very fine-grained, anhedral granular calcite (<0.05mm) predominates. Very small amounts of flaky or anhedral quartz and amorphous silicates, fossil trace, and euhedral or anhedral hematite (after pyrite, 0.1mm) are scattered. Calcite veinlets (<1mm) penetrate the host rock. Recrystallization may not be recognized.
4	A-8061 T	647693	3122782	Aurora F. (Kau XII)	Limestone (fossiliferous).	Grayish chocolate brown, fine-grained, compact, massive, stylolite- structured.	Very fine-grained, anhedral granular calcite (0.02-0.03mm) predominates. Very small amounts of larger calcite (2mm), long prismatic, hexagonal, or anhedral quartz (0.01-0.02mm), spherical or arcuate fossil (Foraminifera) trace (<0.3mm), and subhedral limonitized pyrite (<0.02mm) are scattered. Fossil traces are filled with calcite. Calcite microveinlets (<0.1mm) penetrate the host rock. Recrystallization can not be recognized.

No.	Sample No.	Coordinates			Occurrence	Rock	Macroscopic observations	Microscopic observations
		E	N					
5	A-8072 T	646490	3123843	Aurora F. (Kau XI)	Marl (fossiliferous).	Black, fine-grained, compact, laminated.	Very fine-grained, anhedral granular calcite (<0.02mm) predominates. Small amounts of long prismatic or anhedral quartz (<0.02mm), anhedral chalcidony (<0.02mm), spherical or arcuate fossil (Foraminifera) trace (<0.1mm), and very small amounts of limonite (after euhedral or anhedral pyrite) are scattered. Fossil traces are filled with calcite. A zonal sedimentary structure (lamination) can be recognized by the different grain size of calcite. Oxidized iron stains calcite grains weakly along the laminations. Calcite-pyrite microveinlets (<0.01mm) penetrate the host rock. Recrystallization may not be recognized.	
6	A-8073 T	646443	3123870	Aurora F. (Kau XI)	Marl (fossiliferous).	Black, fine-grained, compact, flaggy.	Very fine-grained, anhedral granular calcite (0.01-0.05mm) predominates. Small amounts of flaky-to-anhedral quartz (0.01-0.03mm), flaky twinned feldspar (0.01-0.03mm), spherical fossil (Foraminifera) trace (<0.1mm), and very small amounts of euhedral-to-subhedral pyrite are scattered. Fossil traces are filled with calcite. Pyrites are partially altered to limonite. A fine sedimentary structure (lamination) is recognized by weak-oxidized iron staining. Calcite microveinlets (0.01-0.1mm) penetrate the host rock. Recrystallization may not be recognized.	
7	A-8074 T	646397	3123923	Aurora F. (Kau X)	Limestone (fossiliferous).	Black, fine-grained compact, stylolite- structured.	Very fine-grained, anhedral granular calcite (<0.01mm) predominates. Small amounts of larger calcite (0.5-1mm), long prismatic, spindle-shaped, hexagonal, or anhedral quartz (0.01-0.02mm), spherical or arcuate fossil (Foraminifera) trace (0.2mm), and very small amounts of anhedral granular pyrite (<0.1mm) and limonite (after pyrite) are scattered. Fossil traces are filled with calcite. Calcite microveinlets (<0.5mm) penetrate the host rock. Recrystallization may not be recognized.	

No.	Sample No.	Coordinates		Occurrence	Rock	Macroscopic observations	Microscopic observations
		E	N				
8	C-1 T	647647	3124258	Aurora F. (Kau IV)	Limestone (recrystallized).	White, fine-grained, saccharoidal, massive, hematite(after pyrite)-spotted, partly pinkish by oxidized iron stain.	Fine-grained, equi-granular anhedral calcite (0.1-0.2mm) predominates showing a granoblastic texture. Very small amounts of anhedral quartz and chalcidony (0.1-0.2mm) fill calcite. Limonite after pyrite is scattered between calcite.
9	C-6 T	648208	3123995	Aurora F. (Kau IV)	Limestone (recrystallized, strongly silicified).	White, coarse-grained, saccharoidal, partly pinkish by oxidized iron stain.	Equi-granular anhedral calcite (1-2mm) fills euhedral-to-subhedral quartz (1-2mm) representing a granoblastic texture. The outer part of quartz shows a zonal texture, and the inner part is a radial aggregate showing a lineage texture. Limonite can rarely be recognized.
10	C-12 T	648055	3125100	Aurora F. (Kau IV)	Limestone (recrystallized).	Dark gray, fine-grained, saccharoidal, compact, massive, limonite(after pyrite)-spotted, penetrated by calcite-limonite veinlets.	Fine-grained, equi-granular anhedral calcite (0.1mm) predominates representing a microgranoblastic texture. Limonite after pyrite (<0.02mm) is sparsely scattered. Calcite-limonite (after pyrite) -fluorite microveinlets (<0.2mm) penetrate the host rock.
11	C-14 T	647485	3124050	Aurora F. (Kau VIII)	Limestone (recrystallized).	White, fine-grained, recrystallized, compact, massive.	Fine-grained, equi-granular anhedral calcite (0.02-0.06mm) shows a microgranoblastic texture. Limonite(after anhedral pyrite, 0.02-0.05mm) is sparsely scattered. An original sedimentary structure (lamination) is recognized by a zonal difference of calcite grain size.
12	C-18 T	647510	3123692	Dyke	Dolerite (altered).	Dark brownish green, compact, altered.	A porphyritic texture with an intergranular-to-interstitial-textured groundmass is observed. Phenocrysts are prismatic-to-tabular euhedral plagioclase (2-4mm) and chlorite pseudomorph after pyroxene (1-2mm). Prismatic plagioclase is fresh and shows an albite-twinning composed of anorthite 50-65%. Tabular plagioclase is strongly sericitized and carbonitized. Groundmass consists of prismatic plagioclase, granular chlorite pseudo-

No.	Sample No.	Coordinates		Occurrence	Rock	Macroscopic observations	Microscopic observations
		E	N				
13	C-21 A T	648273	3124670	Vein	Calcite-quartz-hematite(after pyrite).	Medium-grained, equigranular, massive. Irregular-shaped hematite fills quartz and calcite.	Equi-granular anhedral calcite (<2mm) and sub-hedral quartz (<2mm) show a mosaic texture remarkably. Anhedral hematite (<1mm) surrounds or fills quartz and calcite. Quartz has a lineage texture in its inner part, and includes long prismatic-to-acicular actinolite (<0.2mm).
14	G-8 T	647983	3123785	Aurora F. (Kau VI)	Limestone (recrystallized).	White, coarse-grained, saccharoidal, massive, penetrated by a calcite-fluorite-pyrite vein.	Equi-granular anhedral calcite (0.4-0.8mm) predominates showing a suture-granoblastic texture. Anhedral hematite(after pyrite, <0.5mm) and anhedral granular fluorite (<0.04mm) fill calcite. A calcite-fluorite-pyrite-hematite(after pyrite) vein penetrates the host rock, but the boundary is not clear. Calcite (<2mm) is anhedral, fluorite (<2mm) is anhedral granular, and pyrite (<0.4mm) is also anhedral. Fluorite occasionally includes anhedral pyrite and hematite poikiloblastically.
15	G-20 T	648407	3122893	Aurora F. (Kau X)	Limestone (fossiliferous).	Gray, fine-grained, compact, massive, limonite(after pyrite)-spotted, penetrated by calcite veinlets.	Very fine-grained, anhedral granular calcite (0.01-0.02mm) predominates. Small amounts of long prismatic, flaky, hexagonal or anhedral quartz (0.02mm), and very small amounts of anhedral pyrite (<0.1cm) and spherical or arcuate fossil (Foraminifera) trace (<0.03mm) are scattered. Fossil traces are filled with calcite. Pyrite is partly altered to hematite. Calcite veinlets (<1mm) and microveinlets (<0.01mm) penetrate the host rock. Recrystallization may not be recognized.

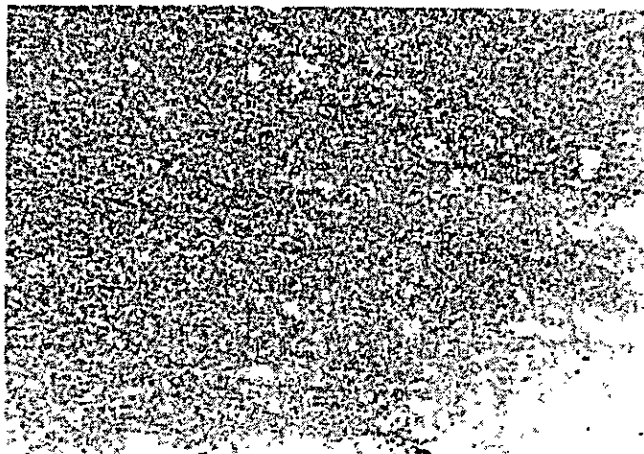
No.	Sample No.	Coordinates		Occurrence	Rock	Macroscopic observations	Microscopic observations
		E	N				
16	G-23 T	647183	3123846	Aurora F. (Kau VIII)	Limestone (recrystallized).	Light gray, partly reddish brown, fine-grained, recrystallized, massive, penetrated by calcite-limonite veins.	Very fine-grained, equi-granular calcite (0.02-0.04mm) predominates showing a microgranoblastic texture. Small amounts of spindle-shaped, hexagonal, or anhedral quartz (<0.3mm), anhedral pyrite (<0.1mm) and hematite (after pyrite) are scattered filling calcite. Calcite-barite veinlets (<4mm) penetrate the host rock. Barite is common and forms a fan-shaped radiating aggregate.
17	G-24 T	647148	3123876	Aurora F. (Kau IX)	Marl (recrystallized).	Brown, brecciated, recrystallized, strongly iron-stained, networked by calcite-limonite.	Very fine-grained, equi-granular calcite (0.02-0.04mm) predominates showing a microgranoblastic texture. Anhedral granular hematitized pyrite (0.04-1mm) is commonly spotted. Marl is brecciated by calcite-limonite networks consisting of anhedral calcite (<0.2-3mm) and filling limonite (after pyrite). Along the cracks of calcite, pyrite (hematite) microveinlets are developed.
18	G-33 T	648365	3125075	Vein	Quartz-pyrite-calcite.	Fine-grained, banded.	Equi-granular subhedral quartz (<0.2mm) predominates representing a mosaic texture. Small amounts of anhedral pyrite and limonite (after pyrite) is included in quartz. Pyrite and limonite are occasionally concentrated to make a pool or a lens. Very small amounts of anhedral calcite fills quartz.
19	G-43 T	647042	3123985	Aurora F. (Kau IX)	Marl (fossiliferous).	Dark gray, fine-grained, compact, laminated.	Very fine-grained, anhedral granular calcite (<0.01mm) predominates. Small amounts of acicular or anhedral quartz (<0.02mm), spherical-to-oval fossil (Foraminifera) trace (<0.2mm), and very small amounts of anhedral granular hematitized pyrite (<0.02mm) are scattered. Fossil traces are filled with calcite. A fine-banded sedimentary structure is clear. Acicular quartz is foliated parallel to the lamination. Calcite-limonite veinlets (<0.2mm)

No.	Sample No.	Coordinates		Occurrence	Rock	Macroscopic observations	Microscopic observations
		E	N				
20	G-70 T	648330	3125047	Aurora F. (Kau IV)	Marl (recrystallized, quartz-calcite- silicified).	Grayish white, fine- grained, compact, recrystallized, dark gray impurity-spotted- or-banded, penetrated by pinkish calcite veinlets.	penetrate the host rock. Recrystallization may not be recognized. Very fine-grained, equi-granular calcite (<0.02mm) predominates. Anhedronal quartz (<0.02mm) is commonly aligned showing an original sedimentary structure. Very small amounts of limonite (after pyrite, <0.2mm) is scattered. Some lenticular pools (<3mm) consisting mainly of calcite (<0.2mm), quartz (<0.1mm) and limonite (<0.1mm) are observed. One of these is composed of diopside, epidote, quartz, calcite, and limonite.
21	G-81 T	647782	3123935	Vein	Garnet-hematite- quartz-calcite- fluorite-gypsum- conichalcite.	Banded as yellowish brown garnet-rich part and quartz-calcite-green copper mineral-rich part.	Garnet-rich part is composed mainly of anhedral irregular-shaped garnet (0.2-20mm). Garnet includes calcite fragments and limonite poikiloblastically. Cracks and partings are remarkably developed in garnet. Quartz-calcite rich part consists of subhedral-to-anhedronal quartz (1-4mm), anhedronal calcite (1-2mm), irregular-shaped garnet (0.1-0.5mm), anhedronal fluorite (1-2mm), anhedronal gypsum (1-2mm), limonite (after pyrite, 2mm), radiating fibrous or colloform conichalcite (<0.5mm). Conichalcite is included in calcite, or is found among other minerals forming a colloform band, and shows an hour-glass extinction. The boundary of garnet- rich part and quartz-calcite-rich part is irregular, and hematite is concentrated. Along the cracks of garnet, quartz and calcite intrude.
22	G-82 T	647782	3123935	Vein	Garnet-quartz- calcite-hematite -conichalcite.	Banded as yellow brown- to-brown garnet-rich part and quartz-calcite- green copper mineral- rich part.	Garnet-rich part is composed of anhedronal granular- to-irregular-shaped garnet (<1.0mm), anhedronal calcite (1-2mm) and small amounts of anhedronal quartz (1-1.5mm). Garnet is occasionally replaced by calcite and quartz along its cleavages. Granular garnet is a relict of the original garnet

No.	Sample No.	Coordinates		Occurrence	Rock	Macroscopic observations	Microscopic observations
		E	N				
23	G-86 A T	647815	3123965	Vein	Garnet.	Yellowish brown-to-yellowish green, massive, limonite-spotted-or-networked.	large crystal. Hematite is concentrated as pools among these minerals. Quartz-calcite-rich part consists mainly of subhedral-to-anhedral quartz (2-8mm). Anhedral calcite (<0.5mm) and limonite(after pyrite, 0.8-2mm) fill quartz. Quartz includes acicular actinolite. Green copper mineral is conchalcite, and is found mainly in quartz-calcite-rich part filling other minerals isolatedly or forming a ring-by-ring atoll structure with limonite.
24	G-88 T	647775	3123912	Vein	Garnet.	Brown-to-yellowish brown, massive, limonite-and-calcite-spotted.	Garnet large crystal (10-20mm) includes wollastonite and actinolite (0.1-0.6mm) poikiloblastically. Garnet shows a zonal structure of crystal growth. Crushing and parting are remarkably developed. Limonite and calcite microveinlets fill the cracks.
25	SLM-1 T	647517	3123377	Dike	Dolerite (altered).	Yellowish brown, compact, altered.	Garnet large crystal (0.5-20mm) includes sheaf-like colorless wollastonite, sheaf-like green actinolite (<1mm), rosetta-formed calcite (1mm), and anhedral quartz (1mm) poikiloblastically. Quartz includes acicular actinolite. Crushing and parting are remarkably developed in garnet, and limonite is disseminated along the cracks. Calcite microveinlets are also developed. Actinolite and chlorite pools (<0.5mm) are found along calcite-quartz veinlets (<0.6mm). A porphyritic texture with an intergranular-to-interstitial-textured groundmass is observed. Phenocrysts are calcite-chlorite pseudomorphs after prismatic or tabular plagioclase (and alkali-feldspar) (<1mm), and chlorite-(calcite) pseudomorphs after subhedral granular pyroxene (<1.2mm). No fresh phenocryst is recognized. The groundmass consists mainly of long prismatic plagioclase (<0.5mm) filled with chlorite pseudomorph after

No.	Sample No.	Coordinates		Occurrence	Rock	Macroscopic observations	Microscopic observations
		E	N				
26	SLM-3 T	647248	3124682	Dike	Dacite (altered).	Light grayish purple, compact but porous. Hornblende, plagioclase and quartz phenocrysts are spotted.	<p>pyroxene (<0.3mm), euhedral magnetite (<0.05mm), and calcite (<0.3mm). Euhedral apatite and acicular biotite (<0.4mm) are also recognized. Plagioclase is strongly altered to calcite, and magnetite is also altered to hematite. Vesicles (<2mm) is filled with calcite. Acicular biotite is likely to have been formed by a thermal metamorphic effect.</p> <p>A porphyritic texture with a devitrified groundmass is observed. Phenocrysts are fragmental quartz (<2.5mm), prismatic or fragmental plagioclase (<2.5mm), subhedral alkali-feldspar (<2mm) and euhedral oxyhornblende (<1.2mm). Plagioclase shows a zonal texture and an albite twinning of anorthite 50-70% component. Oxyhornblende is altered to iddingsite, and the rim is opacitized. The groundmass consists of lath-shaped plagioclase (<0.1mm), plagioclase fragments, apatite, magnetite and glass. Glass is devitrified to form quartz and plagioclase (0.01-0.05mm). Some magnetite is altered to hematite. Very weak chloritization is recognized. A weak flow texture can be seen.</p>
27	SLM-4 DTC	647517	3123717	Dike	Dolerite (altered).	Dark green, compact, chloritized.	<p>A porphyritic texture with an intergranular-to-interstitial-textured groundmass is observed. Phenocrysts are completely replaced by chlorite and calcite. Judging from those shapes, long prismatic-to-tabular phenocrysts are plagioclase and alkali-feldspar, and hexagonal or granular phenocrysts are olivine and pyroxene (augite). The groundmass is composed mainly of long prismatic chlorite pseudomorph after pyroxene, euhedral magnetite and glass. A small amount of apatite and acicular or flaky biotite are also recognized. Plagioclase and glass are almost replaced by calcite and chlorite. Alkali-feldspar is adularia originated from sanidine. Biotite is likely to have been formed by a thermal metamorphic effect.</p>

APX. I-3-(2) PHOTOMICROGRAPHS OF THIN SECTIONS
OF SURFACE SAMPLES



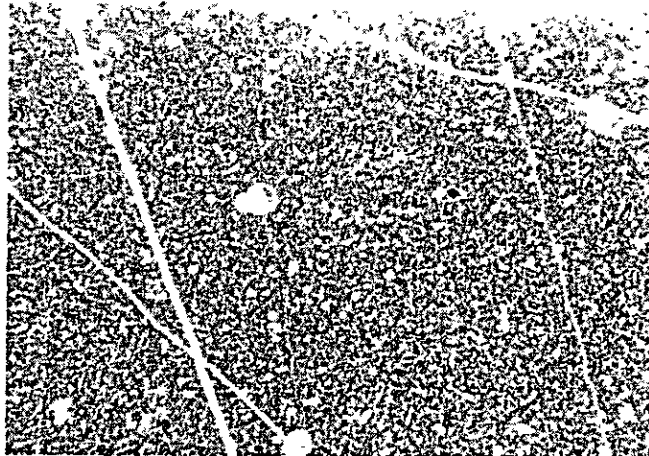
open nicol

0 1 2mm

1) A-7312

Marl.

Lamination is represented by dark gray iron stains. Larger white dots are fossil traces. Small white specks are quartz and some silica minerals. Black specks are hematite.



open nicol

0 1 2mm

2) A-8074

Limestone.

Spherical foraminifera traces are observed. Acicular or rounded white specks are mainly quartz. Calcite micro-veinlets penetrate the host limestone.



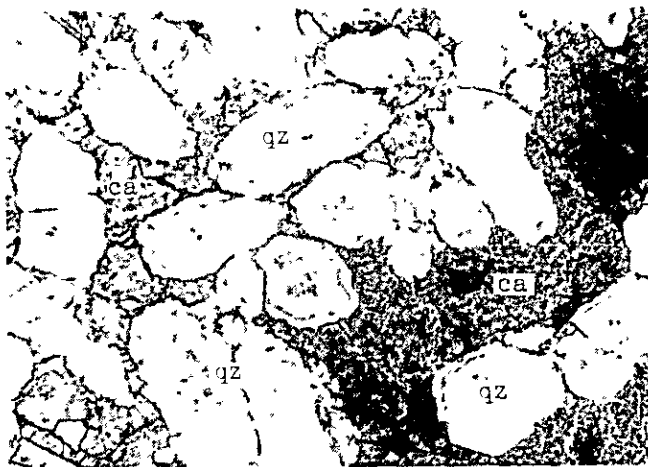
open nicol

0 1 2mm

3) C-1

Recrystallized limestone.

Long prismatic calcite pseudomorphs are sparsely scattered in equigranular calcite. Calcite-fluorite veinlets penetrate the host limestone.
fl: fluorite.



open nicol

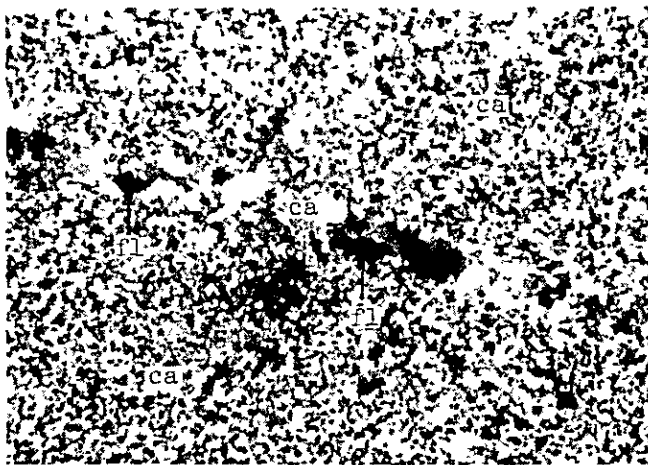
0 1 2mm

4) C-6

Quartz-calcite vein.

Zonal-textured quartz and interstitial calcite. The inner part of quartz shows a radial texture or a lineage texture.

ca: calcite, qz: quartz.



crossed nicols

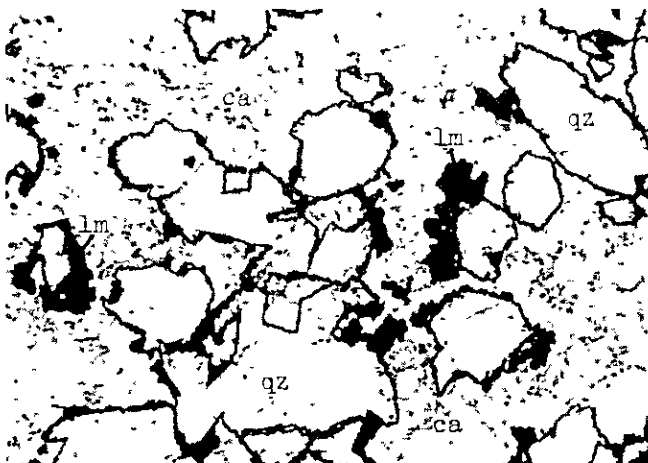
0 1 2mm

5) C-12

Recrystallized limestone.

Equigranular calcite shows a microgranoblastic texture. Calcite-fluorite veinlets penetrate the host limestone.

ca: calcite, fl: fluorite.



open nicol

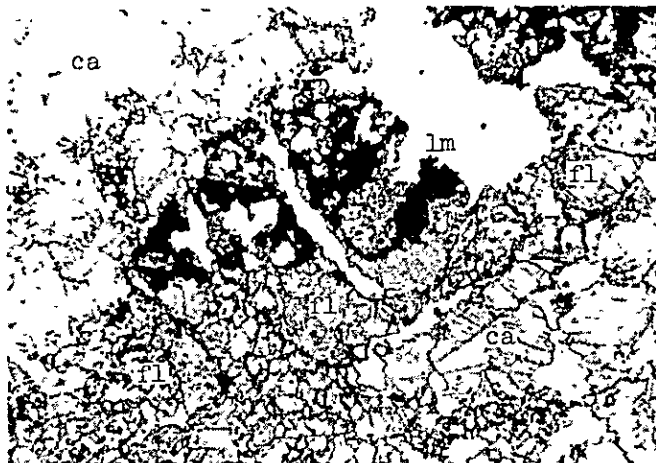
0 1 2mm

6) C-21

Quartz-calcite vein.

Limonite surrounds quartz. Quartz includes acicular actinolite.

ca: calcite, lm: limonite, qz: quartz.



open nicol

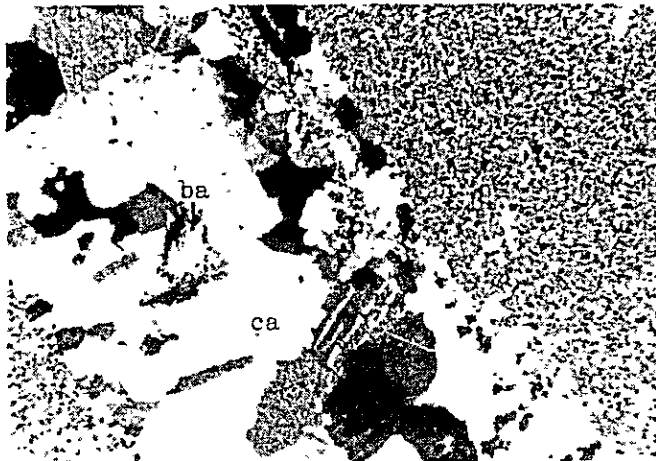
0 1 2mm

7) G-8

Calcite-fluorite-(pyrite) vein penetrating recrystallized limestone.

Crushed fluorite and interstitial limonite. Calcite is also crushed to form granular small grains around larger crystals.

ca: calcite, fl: fluorite, lm: limonite.



crossed nicols

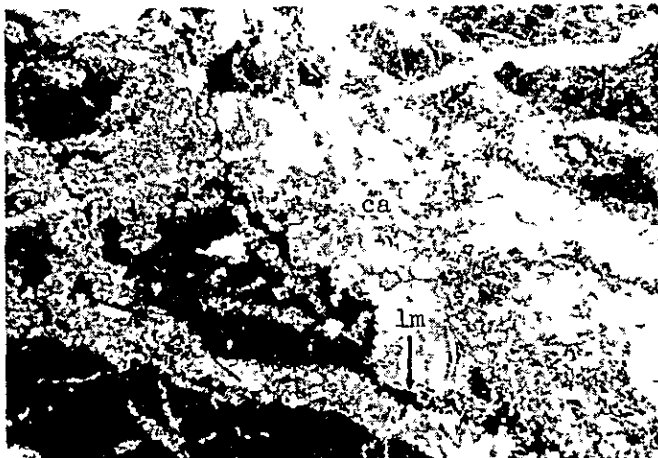
0 1 2mm

8) G-23

Recrystallized limestone penetrated by calcite-limonite-(barite) veinlets.

Acicular-to-hexagonal prisms of quartz are scattered in limestone. Fan-shaped barite is recognized in calcite veinlets.

ca: calcite, ba: barite.



open nicol

0 1 2mm

9) G-24

Brecciated recrystallized marl penetrated by calcite-limonite networks.

Limonite (black) is abundantly concentrated in recrystallized marl.

ca: calcite, lm: limonite.



open nicol

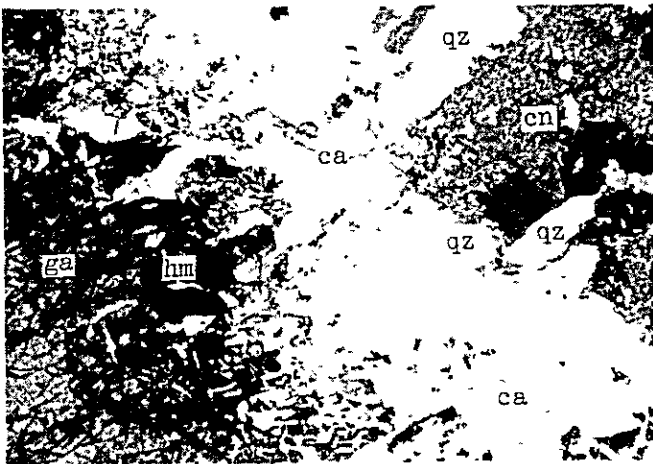
0 1 2mm

10) G-70

Silicified recrystallized marl.

Irregular-shaped quartz is rich. Lamination is visible. Granular epidote is formed in calcite-limonite-quartz lenses.

ca: calcite, ep: epidote,
lm: limonite, qz: quartz.



open nicol

0 1 2mm

11) G-81

Garnet-hematite-quartz-calcite-fluorite-gypsum-conichalcite vein.

Earlier garnet is hybridized by later quartz and calcite. Conichalcite fills quartz and calcite.

ca: calcite, cn: conichalcite
ga: garnet, hm: hematite
qz: quartz.



open nicol

0 1 2mm

12) SLM-1

Altered dolerite.

Mafic minerals are completely replaced by chlorite and calcite. Plagioclase is also replaced by calcite and sericite. Acicular biotite is formed.

bi: biotite, ca: calcite,
ch: chlorite, pl: plagioclase.



crossed nicols

0 1 2mm

13) SLM-3

Altered dacite.

Fragmental phenocrysts of quartz and plagioclase are common. Euhedral oxyhornblende is rare. Glass is devitrified.

hb: oxyhornblende,
pl: plagioclase, qz: quartz.



crossed nicols

0 1 2mm

14) SLM-4

Altered dolerite.

Same as SLM-1.

bi: biotite, ca: calcite,
ch: chlorite, pl: plagioclase

APX. I-4-(1)
MICROSCOPIC OBSERVATIONS
OF POLISHED SECTIONS
&
ELECTRON PROBE
MICROANALYSES
OF SURFACE SAMPLES

No.	Sample No.	Coordinates		Occurrence	Macroscopic observations	Microscopic observations and EPMA
		E	N			
1	A-7274 APE	647873	3123990	Iron oxide-green copper mineral ore (stock pile).	Dark reddish hematite, calcite, and quartz predominate. Light yellowish green irregular-shaped green copper minerals are scattered.	Aggregates of irregular-shaped hematite, goethite and gangue minerals predominate. Copper minerals are fibrous radiating aggregates (<1mm, transparent), irregular-shaped copper oxide (cuprite) and bluish green mineral (<1mm, transparent). Cuprite is grayish white, and shows a strong pleochroism and an anisotropism (reddish brown - dark gray, under crossed nicols). Fibrous radiating aggregates have a green internal reflection, and bluish green minerals have light yellowish green to bluish green internal reflections. These copper minerals are found among gangue minerals. ° EPMA (spot analyses) From "cuprite", Cu and trace Ca were detected, Ca might be an impurity. Therefore, the examined mineral is thought to be a copper oxide. Bluish green mineral contains Cu, minor Si, minor Ca and trace Fe, suggesting that this mineral is chrysocolla or other copper-bearing mineral. The fibrous radial aggregate contains Cu, minor Si, and traces of Zn and Ca.
2	A-8011 APE	647125	3123402	Banded iron oxide-calcite manto.	Black fine-grained hematite predominates. Calcite (and quartz?) is scattered partly. The specimen is porous.	Long prismatic or flaky hematite (<0.005mm) is recognized isolatedly or as an aggregate (<0.03mm) with goethite. In general, the specimen is porous. Gangue minerals might be calcite (irregular-shaped) and quartz (long prismatic). Copper-bearing ? transparent minerals (light green internal reflection) occasionally fill hematite. ° EPMA (spot analysis) Fe and minor Ca, and trace S were detected from a fine-aggregate of flaky hematite. Minor Ca and trace S are thought to be impurities contained in the aggregate.
3	A-8095 APE	647935	3124005	Iron oxide-green copper mineral-calcite manto; the lower part of the manto connects to veins.	Earthy hematite and calcite (and quartz?) fill granular hematite after pyrite. Green copper mineral-pools are spotted.	Flaky or powdery hematite aggregates (<0.05mm), irregular-shaped aggregates (<0.1mm) of copper oxides, native copper, and gangue minerals are recognized. Copper oxides are commonly found among gangue minerals or around hematite in a hematite-rich part. Copper oxides comprise three phases. The first is cuprite, showing

No.	Sample No.	Coordinates		Occurrence	Macroscopic observations	Microscopic observations and EPMA
		E	N			
4	A-80910 APE	648272	3124074	Iron oxide-green copper mineral- calcite vein.	Black granular hematite predominates. Calcite and quartz pools fill hematite.	<p>grayish white color with bluish tint, weak anisotropism and reddish internal reflection. The second is tenorite (paratenorite?) showing grayish brown-to-whitish brown colors and a moderate anisotropism (red-gray color under crossed nicols). The third is thought to be an intermediate phase of cuprite and tenorite (paratenorite?), showing yellow brown color with orange tint, strong pleochlorism and strong anisotropism (dark brown-orange yellow color under crossed nicols). Native copper is rarely scattered as dots (<0.005mm) in cuprite. Tenorite (paratenorite?) surrounds cuprite generally.</p> <p>° EPMA (spot analysis)</p> <p>Cu was detected from cuprite. In the secondary electron image, a slight tone difference is recognized between cuprite and tenorite (paratenorite?), suggesting the difference of copper assay between those two minerals.</p>
5	A-8102 AP	648340	3124095	Iron oxide-green copper mineral vein.	A fine-banded mesh-to-net- work structure of hematite (after pyrite) is remarkable. Light yellow green-to-green, or bluish green copper minerals are observed as pools or as crack-fillings. Bluish azurite is rarely spotted.	<p>Aggregates of flaky hematite and goethite, colloform hematite and gangue minerals are recognized. The colloform hematite is developed around gangue minerals, showing a concentric fibrous texture.</p> <p>° EPMA (spot analyses)</p> <p>Fe and minor Ca from colloform hematite, and Fe, minor copper and minor Ca from goethite were detected. Minor Ca and minor Cu are thought to be impurities contained in hematite and goethite.</p> <p>Irregular-shaped hematite (>0.05mm) forms a mesh-to-network texture with a colloform banding. Some hematite shows a concentric colloform texture, replacing pyrite. Two phases of copper-bearing ? transparent minerals are observed; one has light gray color, and the other has dark gray color. Gangue mineral (and goethite?) micro-veinlets (<0.005mm) penetrate copper-bearing? transparent minerals.</p> <p>° EPMA ... Nil.</p>

No.	Sample No.	Coordinates		Occurrence	Macroscopic observations	Macroscopic observations and EPMA
		E	N			
6	A-8103 APE	648340	3124095	Iron oxide-green copper mineral vein.	Granular hematite(after pyrite)is filled with calcite and quartz. Green copper mineral is observed around hematite and small druses filled with calcite.	Granular hematite(after pyrite)commonly shows an atoll texture. Aggregates of flaky hematite (<0.005mm) represent occasionally a mesh-to-network texture. Irregular-shaped copper oxides (<0.1mm) are rarely observed in gangue minerals. Copper oxides comprise cuprite, tenorite (paratenorite?), and the intermediate phase of those two, as same as A-8095. Copper-bearing transparent mineral is found filling concentric hematite with gangue minerals. ° EPMA(spot analyses) From two hematites, Fe and minor Sb, Pb, Ca, and trace As were detected. Sb might be an impurity or be admixed with hematite as an oxide. Minor Ca, Pb, and trace As might be impurities. From a copper-bearing transparent mineral, Cu, minor Ca, and minor Si were detected, suggesting that this mineral is chrysocholla or other copper mineral. From a gangue mineral, minor Fe, minor Cu, and traces of Pb, Sb, Sn, Ca and Si were detected.
7	A-8104 AP	648248	3124150	Iron oxide-green copper mineral vein.	Granular hematite after pyrite (<8mm) is filled with green copper mineral and calcite. The inner part of granular hematite shows a concentric banding. The specimen is generally porous.	Granular hematite is almost replaced by goethite and gangue minerals. Lenticular hematite relicts show a discontinuous concentric banding texture. Copper-bearing transparent minerals are classified as fibrous grayish one and drak gray one. ° EPMA Nil.
8	A-8105 APE	648273	3124670	Green copper mineral-iron oxide vein.	Granular hematite after pyrite is filled with green copper mineral and calcite. A banded reddish brown hematite and black hematite vein penetrates.	Granular or irregular-shaped hematite(after pyrite, <0.4mm), irregular-shaped or microveinlet-like copper oxides (<0.2mm), granular native copper (<0.02mm), granular or irregular-shaped native silver (<0.02mm), irregular-shaped cerargyrite (0.05mm, transparent), irregular-shaped copper-bearing transparent mineral and gangue minerals are recognized. The banded hematite vein comprise hematite after crushed pyrite. Some hematite shows an atoll texture with gangue

No.	Sample No.	Coordinates E N	Occurrence	Macroscopic observations	Microscopic observations and EPMA
					<p>minerals. Copper oxides and native copper are mostly found nearby a hematite-rich part. Copper oxides are cuprite, tenorite (paratenorite?) and the intermediate phase of those two, as same as A-8095. Native copper is included in cuprite. A mineral zoning in accordance with contained copper quantity is recognized; native copper-cuprite + cuprite-tenorite (paratenorite?) intermediate phase + tenorite (paratenorite?) from the center of copper oxides aggregate. Silver minerals are concentrated among gangue minerals in a copper mineral-rich part. Native silver has glittering bright yellowish white colour. Cerargyrite is dark gray and has dark olive green internal reflection.</p> <p>° EPMA (spot analyses, line scannings, and characteristic X-ray image analysis)</p> <p>From a native silver, Ag, trace S, and trace Ca were detected. Ag, minor Cl, minor I, minor Br, and traces of Cu and Ca were detected from a cerargyrite, confirming that the examined mineral belongs to cerargyrite-bromyrite series. Traces of Cu and Ca is likely to be impurities. From a native copper, only Cu was detected. Cu and minor O were detected from two cuprites, as well as from two tenorites (paratenorite?). Trace Ca is included in those two minerals. From a copper-bearing transparent mineral Cu were detected. Cu-Kα line scannings through gangue mineral, transparent copper-bearing mineral, copper oxides, and native copper show a clear difference of contained copper quantity between those minerals.</p> <p>A Cu-Kα image shows a tone difference between copper oxides and gangue mineral. A spot analysis on hematite detected Fe, minor Sb, minor Ca, and trace Cu. Minor Sb is due to an impurity or a Sb oxide admixed with hematite. Minor Ca and trace Cu are likely to be impurities. From a gangue mineral, probably calcite, Ca and trace Cu were detected.</p>

No.	Sample No.	Coordinates		Occurrence	Macroscopic observations	Microscopic observations and EPMA
		E	N			
9	E-7 AP	647515	3123770	Iron oxide-green copper mineral vein	Predominant granular hematite (after pyrite) is filled with powdery hematite, green copper mineral, calcite, and quartz.	Cubic-to-granular hematite pseudomorphs after pyrite (<2mm) are scattered among admixtures of fine-grained hematite (<0.05mm) and gangue minerals. In the hematite pseudomorphs, cracks are remarkably developed, and a concentric banding is remarkably observed in each parted fragment, suggesting that the original pyrite was strongly crushed. ° EPMA Nil.
10	E-14 AP	646865	3124183	Iron oxide vein.	Very fine-grained black hematite shows an obscure banded structure. The specimen is finely porous.	Very fine-grained flaky hematite (<0.03mm) and microcrystalline hematite compose a banded structure. Pores (<0.05mm) are filled with powdery hematite. ° EPMA Nil.
11	E-38 P	648350	3124348	Iron oxide-green copper mineral vein	Large hematite (after pyrite, 10x20mm) is surrounded by aggregates of granular or elongated hematite (after pyrite), green copper mineral and calcite. The core of large hematite consists of crushed black compact hematite surrounded by fine-banded concentric black hematite and reddish brown hematite. Green copper minerals are mostly found around the large hematite and more outer part.	The core of the large hematite consists of flaky hematite (<0.05mm). The surrounding fine-banded concentric texture is composed of a rhythmic alteration of hematite bands and hematite-gothite-gangue minerals-bands. The remnant part comprise granular crushed hematite (after pyrite, <0.5mm), irregular-shaped copper oxides (<0.2mm) including native copper (<0.05mm), copper-bearing transparent mineral (<0.1mm) and gangue minerals. Copper oxides are cuprite, tenorite (paratenorite?), and the intermediate phase of those two, as same as A-8095. Native copper is included in cuprite as small dots. A zoning is recognized from the center of copper oxides aggregate: native copper → cuprite → cuprite - tenorite (paratenorite?) the intermediate phase → tenorite (paratenorite?). Copper-bearing transparent minerals surround copper oxides. ° EPMA spot analysis. Nil.

No.	Sample No.	Coordinates		Occurrence	Macroscopic observations	Microscopic observations and EPMA
		E	N			
12	G-15 P	647492	3123652	Pyrite small dots in marl.	Pyrite small dots (<1mm) are aligned parallel to the lamination of dark gray marl. Marl is weakly recrystallized and silicified.	Subhedral-to-irregular-shaped pyrite (<0.6mm) is spotted. Pyrite includes irregular-shaped or granular pyrrhotite (<0.02mm) and long prismatic or irregular-shaped gangue minerals (<0.05mm). Alteration can not be recognized. ° EPMA Nil.
13	G-30 AP	648195	3125065	Iron oxide manto.	Porous aggregate of black very fine-grained hematite and reddish brown very fine-grained hematite.	The black hematite-rich part consists of aggregates of irregular-shaped hematite (<0.05mm), and the reddish brown hematite-rich part comprise aggregates of very fine-grained hematite and goethite (<0.04mm). Microcryptocrystalline hematite ring (<0.05mm) bounds each part. Irregular-shaped pores (<0.03mm) are commonly observed. ° EPMA Nil.
14	G-44 APX	646950	3123552	Jarosite-iron oxide manto.	Yellow brown compact jarosite predominates. Dark reddish brown hematite and goethite veinlets-to-networks are observed.	Irregular-shaped or lenticular hematite (<0.05mm) is rarely observed among predominant irregular-shaped or flaky jarosite (<0.02mm, transparent). Some hematite shows a colloform texture. Rare long prismatic-to-flaky pore (<0.02mm) is filled with admixtures of powdery hematite and goethite. Jarosite was identified to be natrojarosite by X-ray powder diffractions and a chemical analysis. ° EPMA Nil.
15	G-82 AP	647782	3123935	Garnet-quartz-calcite-iron oxide-green copper mineral vein.	Cubic hematite pseudomorphs are filled with quartz. Hematite is crushed, and quartz invades as networks. Green copper mineral is concentrated in a quartz-rich part, or around hematite.	Cubic hematite pseudomorphs after pyrite are parted into fragments (<0.7mm), and each fragment shows a lie-sgang texture of alternating hematite bands (<0.01-0.05mm) and gangue mineral bands. Irregular-shaped hematite (<0.1mm) is included in gangue minerals. ° EPMA Nil.

No.	Sample No.	Coordinates		Occurrence	Macroscopic observations	Microscopic observations and EPMA
		E	N			
16	G-85 AP	647885	3124032	Iron oxide-copper mineral vein.	Porous granular or irregular-shaped iron oxides predominate. Pores are filled with quartz, calcite, and reddish brown powdery hematite. Azurite and green copper minerals are rarely spotted.	Hematite bands (0.05mm) show an irregular concentric texture. The core is composed of very fine-grained hematite and goethite. <ul style="list-style-type: none"> o EPMA Nil.

